Technical Report

LABORATORY SIMULATION OF AIRFLOW AND ATMOSPHERIC TRANSPORT-DISPERSION OVER ELK MOUNTAIN, WYOMING

by

K. Kitabayshi,

M. M. Orgill

and

J. E. Cermak

Prepared under

Atmospheric Water Resources Research

Division of the Bureau of Reclamation

Contract Nos. 14-06-D-6455 and

14-06-D-6842

Denver Federal Center

Denver, Colorado

Fluid Dynamics and Diffusion Laboratory

College of Engineering

Colorado State University

Fort Collins, Colorado

July 1971

CER70-71KK-MMO-JEC-65

ABSTRACT

A stably stratified airflow over an isolated mountain was simulated in a wind tunnel and transport-dispersion properties were investigated. Geometric, dynamic and thermal similarity were considered for stably stratified airflows.

The wind tunnel airflow was compared with the field results and also with computer results by Marwitz et al. The agreement of these three systems was fairly good and shallow-water equation system was shown to be a possible mathematical model for this kind of airflow.

Vertical and horizontal dispersion were investigated for a source at ground level on the upwind side of the mountain. The lateral and vertical dispersions were qualitatively simulated in wind tunnel. The vertical dispersion was found to be strongly controlled by the existing inversion. From observations of smoke transport, the blocking effect of the mountain was found to be strengthened by stable density stratification.

TABLE OF CONTENTS

TABLE OF CONTENTS - (Continued)

TABLE OF CONTENTS - (Continued)

LIST OF FIGURES

LIST OF FIGURES - (Continued)

NOMENCLATURE

Symbol	Definition
A	Constant
a	Shape parameter of a hill in Scorer's lee wave solution
b	Shape parameter of a hill in Scorer's lee wave solution
C	Concentration in unit volume
C_D	Drag coefficient
F_1, F_2	Constants in shallow-water solution
f	Coriolis parameter
F_r	Froude number
g	Acceleration of gravity
H	Height of a barrier in shallow-water equation
h	Length parameter for non-dimensional concentration (1km)
h_o	Thickness of air layer in shallow water solution
H_d	Momentum planetary boundary-layer thickness
H_t	Thermal planetary boundary-layer thickness
k	Wave number, or Kármán Constant
K_H	Heat diffusion coefficient
K_M	Momentum diffusion coefficient
L	Monin-Obukhov length scale
L'	Monin-Obukhov length scale in gradient quantities
ℓ	Stability parameter in Scorer's lee-wave equation
M	Non-dimensional barrier height in shallow-water solution
n	Frequency
P	Pressure
P_r	Prandtl number

NOMENCLATURE - (Continued)

Symbol	Definition
Q	Source strength of diffusion material
R_e	Reynolds number
R_i	Richardson number
R_o	Rossby number
S	Non-dimensional wind shear
T	Absolute temperature
t	Time
U,V,W	Horizontal and vertical component of wind velocity
$\overline{U}_g$	Geostrophic wind velocity
u_o	Upstream velocity in shallow water solution
u^*	Friction velocity
x,y,z	Horizontal and vertical coordinates
z_o	Roughness length parameter
$(\ )_\ell$	Laboratory quantity
$(\ )p$	Prototype quantity
α	Proportional constant for friction velocity
β	Non-dimensional potential temperature gradient
ξ	Vertical deviation of streamline
θ	Potential temperature
ν	Kinetic viscosity
ρ	Density
σ_w	Variance of vertical wind component
ϕ	Depth of shallow-water layer

I. INTRODUCTION

1.1 General Statement of the Problem

Wind tunnel simulation of stably stratified airflow over simulated mountainous terrains have been in progress at the Fluid Mechanics and Diffusion Laboratory at Colorado State University for several years. One of the purposes of this work is the simulation of airflow and diffusion over complex or mountainous terrain for possible applications to this type of data programs. Three mountainous areas in the Rocky Mountains have been selected by the Bureau of Reclamation for this type of work. These are the Climax-Eagle River Valley region of central Colorado, San Juan River-Wolf Creek Pass region of southwestern Colorado and the Elk Mountain region of southern Wyoming. Each of these three sites has its own special topographic characteristics. Elk Mountain in this study is different from the others in the sense it is a relatively isolated moutain. Elk Mountain is surrounded by a sagebrush covered plain at an elevation of 7,000 ft msl. The elevation of Elk Mountain is 11,156 ft msl.

For diffusion in mountainous terrain, it was shown by Willis (33) that the existing temperature inversion plays a significant role. It strongly controls the vertical dispersion of passive particles, since the inversion base behave as a ceiling to ascending air-parcels. This kind of temperature inversion usually occurs in the atmosphere through action of ground heating, so that the height of it will depend on topographic features. The effect of the under-lying topography on this inversion base has not been studied extensively.

For the prediction of behavior of a density discontinuity layer in the atmosphere, the shallow-water equation system was shown to be effective by Houghton and Kasahara (11) for airflow over a two-dimensional ridge. Recently it was extended to three-dimensional hills by Spelman (31), Marwitz et al., (20) and Oobayashi (21). Their interests were primarily in hydraulic jump phenomenon in the lee. Marwitz et al., (20) applied this equation system to determine overall airflow character of Elk Mountain flow field. They showed that the mathematical model results agreed fairly well with the field observations. However, the simplifications adopted in that equation system may produce some uncertainty in computed results.

The general purpose of this study was to investigate the airflow and diffusion properties over a scaled topographic model (1:9,600) of Elk Mountain with a physical model that possesses certain similarities to the shallow-water analogy. The model data will be compared with limited field data obtained from the University of Wyoming's Atmospheric Water Resources Research group.

1.2 Objectives of Research

The principal objectives of this work may be summarized as the following:

(1) To develop a laboratory airflow model which would be adequate for estimating the airflow and transport-dispersion characteristics during selected winter events over Elk Mountain and vicinity.

(2) To compare the physical model and field data through the principles of similarity and to determine how well the

physical models can simulate actual atmospheric airflow and transport-dispersion.

(3) To investigate applicability of the shallow-water analogy to the laboratory physical models.

(4) On the basis of field and physical model results examine the feasibility of utilizing model studies of atmospheric transport-dispersion over scaled topographic models for application to weather modification dispersion problems.

1.3 Specific Problem in this Study

Because of the three dimensional character of the terrain in Elk Mountain area, the precise estimation of airflow features by a theoretical model is very difficult except by shallow-water theory. However, up to now we do not know how precisely the shallow water analogy can describe the airflow in three dimensional terrain. The field observations to give the complete description of some particular phenomenon such as the mountain lee wave or hydraulic jump are also difficult and expensive. On the other hand, the wind tunnel study may give a fairly complete description of such phenomenon with little expenditure of time and money. Those results will be reliable when the similarity conditions are properly selected and satisfied in laboratory. Here, we are primarily interested in the change of the mean airflow character produced by the thermal stability, since it governs the transport of passive particles.

1.3.1 The effects of thermal stratification on the blocking of airflow by the mountain - Since in stably-stratified airflow the vertical motion of fluid element is regulated by the restoring force

caused by the density gradient, a change in stream-lines in the horizontal plane will be introduced into the flow field. In other words, the effect of a hill on blocking of airflow will be strengthened by stable stratification.

For two-dimensional airflow, the blocking phenomenon was discussed by Long (18), Kao (13) and briefly by Sheppard (29). Recently, stream-line deflection around a hemisphere was reported by Oobayashi (21) in his airflow using the shallow-water analogy. However, in his work, the ratio of the barrier height and the air layer was decided to one-half so that the results will not be definitive. As suggested by Houghton and Kasahara (11), the ratio of barrier height to air layer is the predominant factor of two dimensional shallow-water flow together with the Froude number.

Since the validity of the shallow-water analogy for airflow over an obstacle will decrease with the increase of the obstacle height because of the vertical homogeneity assumption, the wind-tunnel simulation study will be expected to estimate better the blocking effect in real airflow than the simplified theoretical model. In real airflow over a three-dimensional hill, the vertical homogeneity of flow properties will be somehow obscured, therefore the effectiveness of the shallow water analogy will also decrease because of the three dimensionality. The blocking of airflow is quite important in determining the appropriateness of the source location for cloud seeding operation since it controls the lateral transport of passive particles and vertical movement over the mountain top.

1.3.2 The occurrence of a hydraulic jump and its property - As is well known by shallow-water theory or mountain lee wave theory, high winds occur on the lee side of a hill for stably-stratified atmospheres. By the shallow-water theory, the velocity increase is shown to be dependent on the Froude number, relative height of the hill and also on shape of the hill. However, there remains some uncertainty in application of the theory to airflow over steep topographic slopes, since in the theory the hydro-static equilibrium is assumed. Actually for neutral airflow in the wind tunnel, a separation region is commonly found behind the mountain where the lee slope is steep. However, in the actual atmosphere observation of separation phenomena is not commonly found except in the case of the shedding vortex-trains behind islands which have been observed by cloud photographs taken from satellites.

These latter observations indicate some possibility of separation occurrence in real atmosphere depending on the scale of the mountain. The rotor motion suggested by Scorer (27) can be considered as a mode of separation and it will depend strongly on the stability condition. If the airflow field has discontinuous surface in density or density gradient, the shallow-water analogy seems to be very realistic. In the shallow-water analogy, the down-slope high wind and successive hydraulic jump occur instead of rotor motion suggested by linear perturbation equations for the mountain lee wave. Such that, we can consider the hydraulic jump as a kind of separation. According to Houghton and Kasahara the occurrence and position of the hydraulic jump depends on Froude number and height of the hill relative to depth of fluid layer.

In the shallow-water analogy, a remarkable airflow feature is brought in the velocity field in the lee side. The velocity increases in the lee side from the peak of a hill to the point where the jump exists. By the shallow-water analogy, Marwitz et al.,(20) found a low-wind region in the upwind side of the peak where the wind velocity decreased to nearly 70 percent of the free stream velocity. It was explained by the local increase of the well-mixed layer thickness at that point. On the lee side, a high wind of 125 to 150 percent of the freestream velocity was also reported by them.

The existing downslope wind and hydraulic jump will regulate the vertical dispersion of passive particles near the crest. This is a fairly serious problem in cloud-seeding operation, since we are expecting large vertical dispersion of particles over the peak. In this context, the airflow characteristics near the peak, especially the behavior of existing temperature inversion base may be significant for this problem.

Generally, the hydro-static equilibrium in shallow water equations is appropriate to an airflow with a vertical scale of 10 km and horizontal scale of more than 100 km in atmosphere. Accordingly, in strict sense it is not proper to apply it to a rather small scale air motion like the Elk Mountain simulation study. Therefore, the wind-tunnel study will be helpful to examine the results obtained by shallow-water analogy for a three-dimensional hill.

II. PREVIOUS RESEARCH STUDIES ON AIRFLOW AND DIFFUSION IN MOUNTAINOUS AREA

Many phenomena concerning the effects of topography on airflow have been discovered and investigated up to the present. The mountain lee wave is one of the most well known and has been studied theoretically, observationally in the field and also in the laboratory. However, still some properties such as the relation between wave amplitude and altitude for a variation of stability conditions etc, remain uncertain.

Recently, shallow-water theory for hydraulic wave was utilized to simulate the airflow over a mountain corresponding to the downslope high wind in the lee side. This theory is usually used to simulate cold-and-warm front movements in the atmosphere. In shallow water theory the hydro-static equilibrium is assumed, so that its application to a small scale air motion is usually not completely valid, since in such a phenomenon vertical and horizontal scale of motion are of the same order. Houghton and Kasahara (11) used the theory to describe the airflow over a ridge and explained the occurrence of high winds on the lee side.

2.1 Theoretical Works to the Airflow Over Mountain

2.1.1 Mountain lee wave - Theoretical studies of the two-dimensional mountain lee-wave problem have been accomplished by Long (18), Scorer (26,27) and Queney (24). Long derived an equation which governs the vertical deviation of a streamline from its upstream height because of an existing barrier. His equation is of course two-dimensional and originally nonlinear, however it is reducible to a linear equation under an assumption of constancy of ρU^2 with

height. Then it is solvable analytically. He examined the solution by comparing with experimental results obtained in a water channel in which the density stratification was produced by adding salt to the water.

Scorer derived an equation governing the vertical velocity of fluid element in stably stratified atmosphere. His equation takes the following form after applying Fourier transform for x .

$$\frac{d^2w}{dz^2} + (\ell^2 - k^2)w = 0 \ . \tag{1.1}$$

Here, w is the vertical velocity, k is the wave number for longitudinal direction and ℓ^2 is a quantity related to thermal stability as follows:

$$\ell^2 = \frac{g\beta}{U} - \frac{U''}{U} \ .$$

Here, β is the parameter of potential temperature gradient. He applied this equation for airflow over idealized two-dimensional bell-shaped hill and derived the solution in the following form.

$$\xi = \int \frac{w}{U} dx = \frac{U_1}{U} a^2 \int_0^\infty \exp(-kb+ikx-Uz)dk \ . \tag{1.2}$$

Here, parameters a and b are defined as follows:

a-- a parameter relating to the height of the hill

b-- a parameter for the width of the hill.

In Scorer's equation, the lee wave features are dependent on the associated parameter of thermal stability and vertical profile of

wind velocity. On the other hand, in Long's equation the term related to the velocity profile is not included.

Queney derived an equation by the same approach used by Scorer, but taking into account the Coriolis term which is neglected in Scorer's equation. So that in his equation every term of thermal stability, wave length and Coriolis force is included except the effect of velocity gradient. He solved his equation comparing the effect of each term on lee wave formation. He concluded that a perfect mountain lee wave occurs when the scale of a barrier is nearly equal to the scale represented by the reciprocal of Rossby number. In Queney's equation, however, wind velocity is assumed constant with height i.e., the effect of the velocity profile on lee wave formation is neglected.

By comparing Scorer's and Queney's equations, it is clear that the scales of lee wave considered by them are different. Queney's equation is appropriate to larger scale waves than that by Scorer in the sense that the lee waves are generated by the coupling effect of thermal stability and Coriolis force.

In every work stated above, the fluid is assumed inviscid and non-conductive for heat. This assumption may be reasonable so long as we are concerned with mountain lee wave phenomenon.

The effect of the barrier shape on the amplitude of the lee wave was studied by Wallington (32) using the solution derived by Scorer. He examined mainly the effect of the up-stream slope of the barrier. He concluded that a large amplitude wave occurs at the lower frequencies, if the up-stream slope is rather gentle than

steep. In mountain lee wave problems, however, still many properties remain unknown--particularly the factors governing wave amplitude.

2.1.2 Shallow water theory applied to the airflow over a ridge - The shallow water theory for water waves was also applied to the airflow over a ridge to analyze the downslope high wind on the lee side. Houghton and Kasahara were the first who applied this model to airflow over a ridge. They considered a single-layered model and studied the criteria for existence of a stationary jump. The equations are of the following form:

$$\frac{\partial u}{\partial t} + u\frac{\partial u}{\partial x} + g\frac{\partial \phi}{\partial x} + g\frac{\partial H}{\partial x} = 0 \tag{1.3}$$

and

$$\frac{\partial \phi}{\partial t} + \frac{\partial}{\partial x}(\phi u) = 0. \tag{1.4}$$

Here, x and t denote the space and time respectively, and u and ϕ are the horizontal velocity and the depth of the fluid layer. H is the height of the obstacle which is a given function of x. For the steady-state condition, the system of Eqs. (1.3) and (1.4) admits the following solutions for u and ϕ:

$$\frac{u^2}{2g} + \phi + H = F_1 = \text{const} \tag{1.5}$$

and

$$\phi u = F_2 = \text{const} . \tag{1.6}$$

The two constants F_1 and F_2 are determined by the velocity u_o and the height h_o of the approaching flow far up-stream of the

barrier. Thus,

$$F_1 = \frac{u_o^2}{2g} + h_o \quad \text{and} \quad F_2 = u_o h_o \ .$$

Eliminating ϕ from Eq. (1.5) using Eq. (1.6) and introducing non-dimensional parameter F_{ro} and M and the dimensionless variable U defined by

$$F_{ro} = \frac{u_o}{\sqrt{gh_o}} \ , \quad M = \frac{H}{h_o} \quad \text{and} \quad U = \frac{u}{u_o}$$

we obtain

$$\frac{F_{ro}^2}{2} \bar{U}^3 + \bar{U}(M - \frac{F_{ro}^2}{2} - 1) + 1 = 0. \tag{1.7}$$

This is the relation which governs the steady state solution of U for given initial condition F_{ro} and obstacle conditon M. There exist three real roots of Eq. (1.7) for $M < M^*$, and if the condition

$$M = M^* \equiv \frac{F_{ro}^2}{2} - \frac{3}{2} F_{ro}^{2/3} + 1 \tag{1.8}$$

is satisfied, then two of these roots are equal to

$$\bar{U}^* \equiv F_{ro}^{2/3} \ .$$

They used Eq. (1.7) and showed a chart which describes the relation between F_{ro} and M in connection with the existence of steady hydraulic jump solution (Fig. 3).

Later, Houghton (12) extended this work to a three-layered airflow model and applied it to explain and estimate the high-wind occurrences in the central Rockies near Boulder, Colorado. The agreement of the result with observations was very good and the shallow-water analogy of airflow over the mountain was concluded to be valid.

Another improvement in this model was made by Lavoie (15). He improved the original equations to include the effects of the surface heating and surface drag which were not included in previous works. In his model, the surface drag and heat-flux were introduced in the form proportional to the velocity and temperature difference itself instead of usual gradient forms as follows:

$$\text{drag force} = C_D \frac{\sqrt{u^2+v^2}}{\phi} u$$

and

$$\text{heat-flux} = C_D \frac{\sqrt{u^2+v^2}}{\phi} (\theta_s - \theta) \ .$$

Here, ϕ is the thickness of the well-mixed layer and θ_s is the temperature of the ground surface. In his model, the atmosphere was divided into three layers of different characteristics--

(1) A surface boundary layer of constant momentum flux and heat-flux, extending from the ground upward to heights of 50 m.

(2) A well-mixed dry-adiabatic layer of depth ϕ, having as its upper limit the base of the trade wind inversion.

(3) An upper layer that is neutrally stable in which the motions are adiabatic and no wind shear occurs.

Spelman (31) used this model to estimate the effects of dimensional inhomogeneity of heat, surface roughness and topography. He examined the effect of each inhomogeneity on the airflow separately. According to his conclusion, the surface roughness inhomogeneity cannot have as strong an effect on hydraulic-jump formation as the heat inhomogeneity and topography do.

Oobayashi (21) examined the influence of a hemisphere on the airflow by means of the shallow-water equations. He performed the computation for two different Froude number regions, i.e., subcritical ($F_r < 1$) and super-critical ($F_r > 1$). In his work, a single-layered model was assumed and heat and surface drag terms were not included. According to his results, a strong hydraulic jump existed for the super-critical condition rather than in sub-critical. This is very different from the two dimensional case in which no stationary hydraulic jump can exist for super-critical airflow. He concluded that the blocking effect of the hemisphere was not as great as expected in both the sub-critical and super-critical conditions. However, in his work the height of the obstacle was chosen to be one-half of the inversion base height, so that the conclusion may not be definitive.

Recently, Marwitz et al.,(20) simulated the airflow over Elk Mountain by means of Lavoie's model. They used atmospheric sounding data obtained at Elk Mountain to define the typical stability conditions and the thickness of the well-mixed layer. The height of the well-mixed layer was equated to the height of the planetary boundary layer which was estimated from the potential temperature gradient. The calculated airflow properties were compared with observed data and

the agreement was concluded to be good. They suggested a low-wind region just up-stream of the peak and high wind in the lee side.

As stated by Marwitz et al., the shallow water theory may be the most convenient and appropriate tool to estimate the airflow around a mountain. Since up to the present, the Navier-Stokes equations are still too complicated and time consuming even for solutions to be obtained by computer for a three-dimensional shape.

2.2 Atmospheric Boundary-Layer and Diffusion Properties

Diffusion of particles in the atmosphere has been investigated extensively in connection with air pollution problem.

As is well known, the dispersion of particles is strongly dominated by the turbulence characteristics. Generally, the dilution rate depends not only on turbulence characteristics such as the spectrum profile but also on the sampling duration in the case of a continuous source. In other words, if the sampling duration is long, then the meandering of the plume also becomes effective in determining the mean concentration of the particles. However, in cloud seeding problems we are mainly concerned about the transport, vertical dispersion, horizontal dispersion and concentration of particles at the target area. The number of silver-iodide particles included in unit volume of air is of practical importance for the efficiency of ice-nuclei formation in super-cooled air. Estimation of this efficiency knowledge of the instantaneous concentration.

Since the thickness of the planetary boundary layer and its properties such as the turbulence structure are strongly related to the thermal stability, those relations are summarized in the next section.

2.2.1 Turbulence characteristics and thickness of planetary boundary layer - As is well known, turbulence characteristics in the atmosphere surface layer up to several hundreds of meters are strongly controlled by the thermal stability and the surface roughness of the underlying ground. The vertical component of turbulence is affected especially by ground characteristics. According to the Monin-Obukhov similarity theory, the variance of vertical velocity is usually expressed as follows:

$$\sigma_w = Au^*h'(\frac{z}{L'}) \quad .$$

Here, A is a constant between 1.0 and 1.3, L' is the modified Monin-Obukhov length scale calculated from velocity and temperature gradients, u^* is the friction velocity and $h'(\frac{z}{L'})$ is a universal function of z and L' . Variation of the universal function according to $\frac{z}{L'}$ is given by Lumley and Panofsky (23).

By the same reasoning used for variance of vertical turbulent velocities, the energy spectrum of vertical velocity is expressed by,

$$nSw(n) = \sigma_w^2 G(\frac{nz}{U}, R_i) \quad .$$

Here, R_i is the Richardson number and nz/U is the so-called non-dimensional frequency. The non-dimensional frequency where the energy spectrum profile takes its maximum depends on the Richardson number. It shifts to lower-frequencies in unstable atmosphere and to higher frequencies in stable conditions. According to Hanna (9), this frequency is nearly 0.3 for a near neutral atmosphere.

For the lateral and longitudinal components of turbulence, the situation is a little different since larger scale meteorological conditions and existing hills in up-stream side will contribute to the low-frequency energy spectrum. According to Lumley and Panofsky, low-frequency components of lateral and longitudinal wind fluctuations are almost determined by stability only, although the relating constants are dependent on the geographical characteristics and changes from place to place. These features are valid for lower part of boundary layer only and the properties of upper part of planetary boundary layer are still uncertain.

In regard to the thickness of the planetary boundary layer, several theoretical and observational studies have been made by Rossby and Montgomery (25), Laikhtman (14), Lettau (17) and others. Hanna (10) summarized and examined their equations by comparing with the field data obtained at O'Neill, Nebraska (16). He concluded that for a near-neutral atmosphere the following expression, proposed by Blackadar (5), Lettau and others, gave a fairly good approximation for the momentum boundary-layer thickness:

$$H_d = 0.2\ u^*/f \text{ or}$$
$$= 0.006\ U_g/f\ .$$

Here, u^* is the friction velocity near the ground surface, U_g is the geostrophic wind velocity and f is the Coriolis parameter. For a stably stratified atmosphere, he recommended the following formula proposed by Laikhtman as the thermal planetary boundary-layer thickness,

$$H_t = A\, U_g \frac{1}{\left(\frac{g}{T} \cdot \frac{\Delta\theta}{\Delta z}\right)^{1/2}} \quad .$$

Here, θ is the potential temperature and the vertical gradient was calculated inside of the boundary layer. For the proportionality constant A, Laikhtman suggested 1.3, however, Hanna recommended 0.75 as the best fit for O'Neill data.

In Hanna's work, the momentum boundary-layer thickness H_d was defined as the height where the wind direction first becomes coincident with the geostrophic wind direction. The thermal boundary layer H_t was defined as the height where the vertical gradient of potential temperature first takes a discontinuity. According to Hanna, the average value of H_t in the O'Neill experiment was 1000 m. The planetary boundary-layer thickness is an important parameter for large-scale diffusion problem, since it indicates the region in which the atmospheric turbulence is fairly strong and diffusivity is large.

2.2.2 Particle dispersion in orographic terrain - A comprehensive review of past field studies on transport-dispersion over mountainous terrain has been reported by Orgill (22). Willis (33) reported on the field experiment at Steamboat Springs in Colorado. His experiment was related to the cloud seeding problem and flourescent particles (Zn-S) were used as the air tracer and released generally from the top of a hill of 8,300 feet in elevation. On the downstream side, a valley of 7,000 feet in elevation crosses the flow direction at three miles from the source and the slope rises to peaks of about 10,000 feet

directly from the valley. He reported the airflow and diffusion characteristics in this area as follows:

(1) When an inversion layer existed near the ground, the vertical dispersion of particles was confined strongly to the layer below the inversion.

(2) Horizontal inhomogeneity of airflow caused by the convective motion in day-time strongly influenced the horizontal motion of Zn-S particles.

(3) Sometimes the horizontal wind shear affected the lateral dispersion and made the plume width remarkably large.

(4) Generally, when the bottom of the existing inversion layer was sufficiently high, the vertical dispersion of the particles was fairly rapid.

As seen from these conclusions, the terrain effects coupled with an existing inversion dominates the airflow in mountainous terrain. The effect of ground surface heating was also concluded to be very important.

Smith and Heffernan (30) found that the vertical dispersion was shown very rapid when the existing inversion was sufficiently high. According to their results, the correlation between the cloud top of the particles and the existing temperature inversion height is quite clear.

III. SIMILARITY CONDITIONS

The laboratory simulation of a stably stratified atmosphere was first attempted by Abe (1) in his wind-tunnel study of airflow over Mt. Fuji. His object was the simulation of lee-wave motion and the resultant lenticular cloud formation. He used dry ice to produce a stably stratified airflow in the wind tunnel. He proposed the Reynolds number similarity by using molecular viscosity in the model flow and an eddy viscosity for the prototype. This similarity concept may be valid so long as we are concerned about large-scale air motion such that the surface boundary layer has no significant effects on the main phenomenon.

At Colorado State University, several works (6), (7), (8), (22) have been done in wind tunnel simulation of stably-stratified airflow over geographical area. By these works the similarity criteria has been established for stably stratified airflow.

3.1 Similarity Conditions for Airflow in Turbulent Boundary Layer

The governing equations for continuity of momentum and energy are (neglecting the compressibility):

$$\frac{\partial u}{\partial t} + u\frac{\partial u}{\partial x} + v\frac{\partial u}{\partial y} + w\frac{\partial u}{\partial z} - fv = -\frac{1}{\rho}\frac{\partial P}{\partial x} + \frac{\partial}{\partial z}\{(K_m + \nu)\frac{\partial u}{\partial z}\}$$

$$\frac{\partial v}{\partial t} + u\frac{\partial v}{\partial x} + v\frac{\partial v}{\partial y} + w\frac{\partial v}{\partial z} + fu = -\frac{1}{\rho}\frac{\partial P}{\partial y} + \frac{\partial}{\partial z}\{(K_m + \nu)\frac{\partial v}{\partial z}$$

$$\frac{\partial w}{\partial t} + u\frac{\partial w}{\partial x} + v\frac{\partial w}{\partial y} + w\frac{\partial w}{\partial z} = -\frac{1}{\rho}\frac{\partial P}{\partial z} - g\frac{\Delta t}{T_o}$$

$$\frac{\partial T}{\partial t} + u\frac{\partial T}{\partial x} + v\frac{\partial T}{\partial y} + w\frac{\partial T}{\partial z} = \frac{\partial}{\partial z}\{(K_H + k)\frac{\partial T}{\partial z}\}$$

Here, by introducing non-dimensional quantities as follows:

$$u^* = \frac{u}{\overline{U}}, \quad v^* = \frac{v}{\overline{U}}, \quad w^* = \frac{w}{\overline{U}}, \quad P^* = \frac{P}{\rho\overline{U}^2}, \quad \theta^* = \frac{\Delta T}{\Delta T_o},$$

$$x^* = \frac{x}{L}, \quad y^* = \frac{y}{L}, \quad z^* = \frac{z}{L}, \quad t^* = \frac{t}{L/\overline{U}},$$

$$K_M^* = \frac{K_M + \nu}{K_{Mo}}, \quad K_H^* = \frac{K_H + k}{K_{Ho}}, \quad R_e = \frac{\overline{U}L}{K_{Mo}}, \quad P_r = \frac{K_{Mo}}{K_{Ho}}$$

$$R_i = \frac{g\Delta t_o}{To\overline{U}^2}\Delta z, \quad R_o = \frac{\overline{U}}{fL},$$

the original equations are rewritten,

$$\frac{\partial u^*}{\partial t^*} + u^*\frac{\partial u^*}{\partial x^*} + v^*\frac{\partial u^*}{\partial y^*} + w^*\frac{\partial u^*}{\partial z^*} - \frac{1}{R_o}v^* = -\frac{\partial P^*}{\partial x^*} + \frac{1}{R_e}\frac{\partial}{\partial z^*}(K_M^*\frac{\partial u^*}{\partial z^*})$$

$$\frac{\partial v^*}{\partial t^*} + u^*\frac{\partial v^*}{\partial x^*} + v^*\frac{\partial v^*}{\partial y^*} + w^*\frac{\partial v^*}{\partial z^*} + \frac{1}{R_o}u^* = -\frac{\partial P^*}{\partial y^*} + \frac{1}{R_e}\frac{\partial}{\partial z^*}(K_M^*\frac{\partial v^*}{\partial z^*})$$

$$\frac{\partial w^*}{\partial t^*} + u^*\frac{\partial w^*}{\partial x^*} + v^*\frac{\partial w^*}{\partial y^*} + w^*\frac{\partial w^*}{\partial z^*} = -\frac{\partial P^*}{\partial z^*} - R_i\theta^*$$

$$\frac{\partial \theta^*}{\partial t^*} + u^*\frac{\partial \theta^*}{\partial x^*} + v^*\frac{\partial \theta^*}{\partial y^*} + w^*\frac{\partial \theta^*}{\partial z^*} = \frac{1}{R_e P_r}\frac{\partial}{\partial z^*}(K_H^*\frac{\partial \theta^*}{\partial z^*}).$$

Therefore, the laboratory airflow has to satisfy the following five conditions for complete simulation:

(1) geometrical similarity

(2) Richardson number similarity

(3) Reynolds number similarity

(4) Prandtl number similarity

(5) Rossby number similarity.

As well known, Rossby number similarity is usually not an essential requirement as long as the horizontal scale of the phenomenon is less than the order of 100 km. Prandtl number similarity will be satisfied if air is used in the laboratory as the fluid, since the Prandtl number is nearly equal to unity for both laminar and turbulent flow as long as the thermal effect is moderate.

3.2 Airflow Similarity in Non-Stratified Boundary Layer

In neutral airflow, since the Richardson number is zero, both the geometrical similarity and the Reynolds number similarity are required to be satisfied in the laboratory. If the scale of the topographic model is equal in the horizontal and vertical, geometrical similarity is satisfied.

The eddy diffusivity at some reference height z_1 in the boundary layer is given as follows:

$$K_m = ku^*z_1 \quad .$$

Then the Reynolds numbers in the laboratory and in the field when both flows are turbulent are (neglecting molecular viscosity):

$$R_{e\ell} = \frac{\overline{U}_\ell L_\ell}{k u_{*\ell} z_{1\ell}} \quad , \quad R_{ep} = \frac{\overline{U}_p L_p}{k u_{*p} z_{1p}} \quad .$$

By equating both the Reynolds numbers, the following conditions will be derived:

$$\frac{\overline{U}_\ell}{\overline{U}_p} = \frac{u_{*\ell}}{u_{*p}} \quad .$$

Here, if the geometrical similarity is satisfied and the surface roughness is adjusted properly, then, by well known log-profile, $\frac{\overline{U}}{u_*} = \frac{1}{k} \ell n \left(\frac{z_1}{z_o}\right) = \alpha$. Therefore, the friction velocities are expressed by $u_{*p} = \alpha \overline{U}_p$, $u_{*\ell} = \alpha \overline{U}_\ell$ and the required condition $\frac{\overline{U}_\ell}{\overline{U}_p} = \frac{u_{*\ell}}{u_{*p}}$ will be satisfied for any freestream velocity as long as the wind tunnel boundary layer is turbulent and fully developed. Therefore, in neutrally stable airflow the required similarity condition is only geometrical similarity. The Reynolds number similarity may be replaced by the condition that the boundary layer is fully developed and an equilibrium state is attained.

3.3 Airflow Similarity in Stably Stratified Boundary Layer

In a stably stratified boundary layer, as long as the airflow is turbulent and stability is moderate, the eddy diffusivity may be

expressed as follows (by Lumley and Panofsky):

$$K_m = \frac{1}{S} ku^*z \quad .$$

where S is the ratio of the eddy diffusivities in neutral and non-adiabatic airflow and related to non-dimensional stability parameter as follows:

$$S = \phi_1(z/L) \quad .$$

Where L is the Monin-Obukhov scale length calculated from fluxes of heat and momentum. By comparing wind tunnel results and field data, Arya and Plate (2) concluded that the gradient Richardson number and non-dimensional stability parameter z/L would be related by a common universal function. Therefore, the function $\phi_1(z/L)$ might be expressed by the gradient Richardson number also. If we denote this function by $\phi_4(R_i)$ such as,

$$S = \phi_1(z/L) = \phi_4(R_i) \quad .$$

Then, the eddy diffusivity in stratified boundary layer is

$$K_m = ku_*z_1/S = ku_*z_1/\phi_4(R_i) \quad .$$

Therefore, the Reynolds number similarity is

$$R_{e\ell} = \frac{\overline{U}_\ell L_\ell \phi_{4\ell}(R_i)}{ku_{*\ell} z_{1\ell}} = Rep = \frac{\overline{U}_p L_p \phi_{4p}(R_i)}{ku_{*p} z_{1p}}$$

Finally as the freestream velocity condition we obtain

$$\frac{\overline{U}_\ell}{\overline{U}_p} = \frac{u_{*\ell}}{u_{*p}} \frac{\phi_{4p}(R_i)}{\phi_{4\ell}(R_i)}$$

Since, by Arya and Plate, the function $\phi_{4\ell}(R_i)$ was shown to agree quite well with field condition $\phi_{4p}(R_i)$ Reynolds number similarity is automatically satisfied by adjusting Richardson number. Thus, as long as the flow is turbulent and an equilibrium state is attained, the required similarity conditions in stably stratified boundary layer are the geometrical similarity and Richardson number similarity.

In a practical sense, however, it is not easy to produce a fully developed strongly stratified stable airflow in wind tunnel, since in order to produce a strong stratification, the wind velocity must be low. For this case, the airflow becomes nearly laminar and the previous similarity relations cannot be applied to the problem.

Batchelor (4) discussed the similarity condition for small scale motion in non-viscous thermally stratified atmosphere. He concluded that the Richardson number is a local similarity index and is the only similarity condition which characterizes the airflow if the airflow is non-viscous and the vertical scale is small enough.

Cermak and Peterka (6), concluded that the three conditions (1), (2), and (3) are sufficient for similarity of stable airflow. They used the Reynolds number similarity proposed by Abe in which the eddy viscosity was replaced by molecular viscosity in the model flow. This assumption was shown to be met by airflow in the wind tunnel, since the turbulence was suppressed by strong thermal stratification

and the airflow was nearly laminar except at the place where the topography was highly irregular such as the lee side of a hill. Following these previous works, topographical similarity, Froude number similarity and Richardson number similarity are considered mainly and Reynolds number was examined in this study.

Since the horizontal scale of the airflow is more than 20 km and the vertical scale is nearly 3 to 4 km, the usual gradient Richardson number may be meaningless to describe the total character of the airflow in this model. Thus the bulk Richardson number is adopted as the similarity index as follows:

$$R_i = \frac{g}{\bar{\theta}} \frac{\Delta\theta}{U^2} z \quad .$$

If the flow field consists of several layers in which the potential temperature is different from each other and our main interest is the characteristic movement of these discontinuity surfaces rather than the small scale structure of the airflow, then another similarity condition based on this discontinuity height should be added. Therefore, we also adopted the Froude number similarity based on the well-mixed layer height as follows:

$$F_r = \frac{U}{\sqrt{gh}} \quad .$$

The Froude number similarity requires the wind tunnel velocity as,

$$U_\ell = U_p \sqrt{\frac{h_\ell}{h_p}} \quad .$$

Since U_p is nearly 15 to 20 m/s, the wind tunnel velocity U_ℓ is 15 to 20 cm/s by the above condition. By this Froude number similarity, Reynolds number similarity could be excluded. However, the Reynolds number similarity is also satisfied by taking the molecular viscosity in the wind tunnel instead of eddy viscosity.

IV. EXPERIMENTAL RESULTS

4.1 Results of Field Measurements

The field observations at Elk Mountain have been made by the University of Wyoming Atmospheric Water Resources Research group. The test site is located nearly 15 km southwest of Elk Mountain peak. The field soundings have been done mainly in winter time for westerly wind conditions. The observations consisted of rawin-sonde, radar tracking of constant-pressure balloons and concentration measurement of ice-nuclei. By rawin-sonde, vertical profiles of wind velocity and temperature were obtained. The ice-nuclei concentration was measured at the mountain peak only, so that some uncertainty remains in vertical dispersion.

4.1.1 Wind velocity and temperature profiles - The vertical profiles of velocity and temperature were obtained from the rawin-sonde sounding data. Since generally, the individual field sounding datum is influenced by meso and synoptic scale weather conditions and cannot be typical for any reference place, so that we have to eliminate these special influences from each individual datum by some appropriate menas. In this study, the typical atmospheric condition for westerly wind is obtained by taking the average of several sounding data. In Fig. 4, the mean potential temperature profile of ten soundings is shown. As is easily seen, the temperature gradient has a clear discontinuity at nearly 1 km above the ground. According to Hanna, we can consider this height as the upper boundary of the thermal planetary boundary layer. This height agrees with Hanna's estimation of planetary boundary layer by O'Neill data. The mean

potential temperature gradient is nearly 2° K/km inside of boundary layer and 4° K/km in the upper stable layer. This remarkable difference of temperature gradient in two layers may support the validity of the shallow water analogy to the real airflow. By individual soundings, the boundary layer height by temperature gradient varies between 700 and 2000 m.

The average vertical profiles of wind velocity and wind direction are shown in Fig. 5. The averages were computed from ten sets of data. In the wind velocity profile, the boundary layer height is not so clearly definable as in the temperature profile. The wind velocity becomes constant first at 1 km and wind direction takes a constant value at 1.5 km, so that we may consider the boundary layer thickness in the momentum field between 1.0 to 1.5 km.

The bulk Richardson number based on the height scale 2 km and Froude number on the base of the planetary boundary layer thickness (temperature inversion height) are completed from the following relations:

$$R_{ib} = \frac{g}{\bar{\theta}} \frac{\Delta\theta}{\bar{U}^2} z \quad ,$$

$$F_r = \sqrt{\frac{\bar{U}}{gh}}$$

where $\bar{\theta} = 300^{\circ}$ K, $z = 2$ km, $\Delta\theta = 6^{\circ}$K, $U = 15$ m/s, $h = 1$ km . So that the bulk Richardson number is 1.7 and Froude number is 0.15.

4.1.2 Airflow over mountain - The typical constant-pressure balloon traces in vertical and horizontal planes are shown in Figs. 6 and 7. As easily seen in Fig. 6, the down-slope high wind occurs

occasionally but not always, i.e., in Fig. 6-1, the down-slope high wind seems to exist in the lee side and it will cause the hydraulic jump at the more downstream place. Since the hydraulic jump depends on the Froude number and relative barrier height, the density gradient condition might not meet with the required condition in the case of Fig. 6-2. In Fig 6, the longitudinal velocity changes of balloons are also shown. As easily seen, for the case of Fig. 6-2, velocity clearly decreases in the lee side. However, in Fig. 6-1 it does not decrease but maintains nearly the same velocity at the crest. The constant-pressure balloon data in Elk Mountain usually show a high wind region around the crest. This feature is not in agreement with the computer results. In the computer work by Marwitz et al., (20), the existence of a low-wind region just upstream of the crest is reported.

In Fig. 7, horizontal traces of constant-pressure balloons are shown. If the balloon traces are considered to be streamlines the horizontal airflow seems to be influenced slightly by the existing mountain. In short, the blocking effect of the mountain is not as strong as might be expected. However, the balloon data are not sufficient and since the horizontal wind shear also affects the data, therefore, conclusive discussion is difficult for this problem.

4.1.3 Streamline distribution over the mountain - Streamline distribution over Elk Mountain as estimated from aircraft observations is shown in Fig. 8-1 as reported by Marwitz et. al., (20). The existence of an atmospheric "hydraulic" jump and associated downslope wind on the leeside of Elk Mountain is strongly suggested in Fig. 8-1. Computer simulation of the streamlines over Elk Mountain is shown in

Fig. 8-2. Generally, there is good qualitative agreement between the observations and computer results. However, in the upstream side of the crest, the vertical deviation of the streamlines by the computer model appears a little larger than the field result.

4.2 Wind Tunnel Results

The wind tunnel experiments were divided into two phases. The first phase considers the flow properties and diffusion in non-stratified airflow and the second considers the measurements in stably stratified airflow.

In neutral airflow, velocity profiles and surface wind directions were measured over the model as the flow field measurements. For the stably stratified case, temperature profiles and velocity profiles were investigated. Since in stably stratified airflow, the density stratification had strong effects on the velocity field, several devices were tried and used to control the airflow and to produce similarity with the prototype data.

4.2.1 Non-stratified airflow

(a) Airflow characteristics

The measurements of flow characteristics and diffusion in non-stratified airflow were studied for a freestream velocity of 9 m/s. The boundary-layer thickness (defined as 95% of freestream velocity) was nearly 30 cm.

As is well known, the velocity profile near the ground over homogeneous terrain is approximated quite well by a so-called log-profile. However, if the boundary is not flat, especially in the sloping terrain, the velocity profile deviates from the logarithmic law. Large deviations were caused by separation from ridge lines along the crest of Elk Mountain.

In neutral airflow over the Elk Mountain model, the velocity profile in the flat plain upstream of the mountain was found to be nearly logarithmic. However, at the upstream slope and lee side of the crest, the velocity profiles cannot be expressed by the logarithmic law. On the upstream slope, the velocity near the surface increases and becomes a very flat profile. In the lee side, the velocity decreases near the surface because of the existing separation. The wind velocity on the upstream slope at 6 cm (about 600 m in prototype scale) above the surface increases to 115 percent of the velocity at the same height on the flat plain and it decreases to 50 percent in the lee side. In Fig. 11, the velocity profiles along lines B and C are shown. As is easily seen, a separation region exists in the lee side. However, such a separation is not usually reported for a sufficiently high hill in the real atmosphere.

Streamlines around the mountain estimated from the miniature bi-directional vanes observation is shown in Fig. 12. A remarkable deflection of streamlines is clearly seen in the lee side of the mountain where a separation is found by velocity measurements. The blocking effect of the mountain is fairly strong in the steep south-west valley but generally not so apparent in other places. The

picture of a smoke streak also showed a fairly wide plume fluctuation but not a strong blocking effect.

(b) Dispersion of Krypton-85

The contour-lines of Krypton-85 concentration at ground level in neutral airflow is shown in Fig. 13 for source point 6. As is easily seen, the plume axis does not deviate largely from the freestream direction. The lateral deviation of the plume axis from the line passing through the source point in the free-stream direction is nearly 12 cm (about 1.2 km in prototype scale) at 208 cm (20 km) downstream.

The dispersion width of Krypton-85 defined by the distance from the plume axis to the point where the concentration decreases to 10 percent of the concentration at the plume axis is nearly 28 cm (2.8 km in prototype) at 104 cm (10 km) downstream of the source. This is equivalent to 16 degrees in plume angle and is a little larger than the field observation result--about 10 degrees according to Ref. (3). But their plume width was defined by the width where ice nuclei concentration decreased to ten times of background concentration so direct comparison is difficult. According to Smith and Heffernan (30), the plume width at 10 km downstream was usually between 3 to 5 km, but the definition of plume width was not clearly defined in their paper. Also, their observations were carried out in mountainous terrain.

In Fig. 14, the vertical contour-lines of Krypton-85 concentration are shown. In the neutral case, the dispersion was farily rapid and it increases further in the lee side. This may be because of increasing turbulence caused by separation. The plume-dispersion scale defined

by the height where the concentration decreases to one-tenth of the ground value becomes 20 cm (about 2 km) at 208 cm (20 km) from the source. By Smith and Heffernan, the top of the plume at 10 km downstream reached 1300 to 1500 m and 1500 to 1800 m at 30 km. Their results show that as long as the temperature inversion base is high the plume spread is fairly rapid.

4.2.2 Stably stratified airflow and diffusion - In stably stratified airflow in the wind tunnel, the ambient air was heated up to 32^{o} C and air near the floor was cooled by dry ice blocks and refrigeration of the floor plate. However, the model surface temperature was higher than the air and a thermally unstable airflow layer existed near the surface. This type of thermal stratification is qualitatively similar to the real atmosphere in daytime. The wind velocity was determined to be nearly 20 cm to meet the similarity requirements for equality of the Froude number.

(a) Temperature profiles over the mountain

In a stratified airflow if the vertical scale of the motion is sufficiently small compared with horizontal scale, then the similarity factor of small scale airflow characteristics such as velocity profiles or turbulence properties will be Richardson number as discussed by Batchelor. However, if the flow field has a discontinuity surface in fluid density or in density gradient and we are interested in large-scale air motion, then the Froude number based on the height of the discontinuity surface may be a governing factor together with a bulk Richardson number. In this simulation study, the airflow

velocity and upstream conditions were arranged to satisfy the bulk Richardson number similarity and also Froude number similarity.

The temperature profiles along measuring lines B and C are shown in Figs. 15-1 and 15-2, together with the iso-temperature lines. The entire flow field can be divided into three layers with different thermal stability as follows:

(1) Unstably stratified flow layer from the model surface to nearly 2 cm (about 200 m in prototype) above the surface, where the airflow temperature decreases upwards. This layer was produced due to the temperature difference between the air and the model surface.

(2) Near neutral stability layer above the unstable layer which extends up to nearly 10 cm (1000 m) above the model surface. In this layer, the air temperature is nearly constant with height.

(3) The top layer where the airflow is stably stratified with a temperature gradient of about $1.2^{o}c/cm$.

These flow field structures are very similar to the field. Actually, except for the height of the layers, it has the same structure with the model atmosphere as simplified by Lavoie in his shallow-water model. The height of the neutral airflow layer in the wind tunnel is 1000 m in prototype scale, and it agrees quite well with the average height of 1000 m for the field conditions.

Since in stably stratified airflow, the flow was nearly laminar except the well mixed layer, we can assume approximately the constant temperature lines equivalent to streamlines. Along the measuring line B, the vertical deviations of the constant temperature lines are

fairly small and they are nearly parallel to each other. This supports the assumption of negligible heat diffusion along this line. On the line B, the hydraulic jump seems to be weak. This is reasonable since the lee side slope is gentle along this line. The flow visualization by smoke also proved this weak hydraulic jump along line B. Along line C, where the lee side slope is steep, the vertical deviations of constant temperature lines are fairly rapid. The figure clearly shows the hydraulic jump on the lee side. There, the temperature gradient becomes small because of the strong mixing produced by the hydraulic jump. The flow visualization (Fig. 23) also shows the existing hydraulic jump. The upper level constant temperature line elevation upstream of the peak does not change significantly due to the underlying topography. This implies the existence of a blocking effect. Generally, the constant temperature line distribution around the mountain shows a fairly good agreement with the iso-thermal lines in the field results.

The height of the temperature-inversion base increases slightly at high elevation points and decreases rapidly on the lee side. The contour lines of the temperature inversion base are shown in Fig. 16. This height is comparable to the well-mixed layer height in the computer model by Marwitz et al., (20), and it will indicate the upper limit of dispersion of passive contaminants released from the ground. As is easily seen, the height change of the inversion base at the upstream slope is quite samll, but it decreases remarkably in the lee side. However, generally, the vertical deviation of the inversion base in wind tunnel is smaller than that predicted by the computer results of Marwitz et al.

The Froude number based on the inversion height is 0.2 and is nearly equal to the field value.

(b) Velocity profiles and velocity changes along measuring lines

The vertical profiles of wind velocity and the velocity change along lines B and C at 6 cm (about 0.6 km) from the surface are shown in Fig. 17 and 18, respectively. The velocity change in stably stratified airflow is larger than the neutral airflow. In stable case, high wind velocity is usually observed near the ridge of the mountain. However, in the lee side of the mountain a remarkable difference exists between velocities on lines B and C. Along line B, the velocity does not decrease on the lee side and keeps almost the same velocity at the ridge. Along line C on the other hand, it decreases from 160 percent of the upstream velocity at the ridge to 105 percent on the lee side. The highest velocity in the wind tunnnel experiment was found near the ridge along line B and reached 170 percent of the upstream velocity.

(c) Diffusion in stably-stratified airflow

In Figs. 19 and 20, the contour-lines of Krypton-85 concentration in horizontal and vertical planes are shown. The horizontal contour-lines were drawn from the ground level concentration and the vertical one shows the plume section along the plume axis. By comparing the horizontal distributions for neutral and stable cases, the strengthened effect of the blocking in stable airflow is clear. However, because of the existing neutral layer near the surface, the horizontal dispersion in stably stratified airflow does not change significantly in magnitude from the neutral case.

In regard to vertical dispersion, a significant difference from the neutral airflow occurs in stable cases. The vertical height of the plume decreases rapidly over the lee side of the mountain, in contrast to the neutral stability case in which the plume height continues to increase. This plume behavior follow from the flow characteristics on the lee side. The plume dispersion is restricted to a region less than 12 cm (about 1.2 km in prototype scale) in height over the entire model. The upper boundary of the plume is closely related to height of the inversion base, although it was observed to be slightly higher. The nondimensional concentration at the ground in stable airflow is nearly five times larger than for the neutral case.

(d) Flow visualization by smoke

In Figs. 21 and 22, the plume traces obtained by smoke visualization pictures are shown. The blocking effect of the mountain is quite strong for sources north and south of Elk Mountain. For the sources located just upstream of Elk Mountain, deflection of the plume axis from the freestream direction is rather small, but the dispersion is quite large in the lateral direction.

In Fig. 23, side views of smoke flow are given. We can clearly see the downslope wind and resultant hydraulic jump on the lee side, however, no apparent indication of the occurrence of a mountain lee wave was detected.

V. COMPARISON OF LABORATORY AND FIELD EXPERIMENTAL RESULTS

5.1 Airflow Similarity

In the wind tunnel, the freestream velocity was selected to give Froude number similarity,

$$\frac{F_{rp}}{F_{r\ell}} = \frac{\dfrac{\overline{U}_p}{\sqrt{gh_p}}}{\dfrac{\overline{U}_\ell}{\sqrt{gh_\ell}}} = 1 \quad .$$

From this condition, the following relation is obtained,

$$\left(\frac{\overline{U}_p}{\overline{U}_\ell}\right)^2 = \frac{h_p}{h_\ell}$$

The above equality simplifies the similarity condition for bulk Richardson number as follows:

$$\frac{\Delta T_\ell}{T_\ell} = \frac{\Delta\theta_p}{\theta_p} \quad .$$

Since the mean airflow temperature in the wind tunnel and in the field are nearly equal to each other, the temperature difference distributions are required to be similar in both airflows by Richardson number similarity. In Fig. 24, bulk Richardson number profiles in laboratory and in field are displayed. The coincidence of both profiles is fairly good in well mixed layers. However, in the upper layer, the wind tunnel Richardson number is nearly twice as large as the field value.

The Froude number based on the temperature inversion height is 0.15 and 0.20 in field and wind tunnel, respectively.

The velocity change along streamlines qualitatively agree with that found from the field observations. The high wind speed observed at the ridge of the mountain decreases as motion proceeds over the lee side (Fig. 17). These features of flow-velocity changes seem to be different from the computer results of Marwitz et al., (20). The flat velocity profiles in the wind tunnel are in good agreement with the vertically homogeneous flow assumed in the shallow-water equations.

The blocking effect of the mountain is clearly evident in the wind tunnel. For the smoke source north to the Elk Mountain, the lateral deviation of the plume axis from the free streamline reaches nearly 15 cm (1.5 km in prototype scale), (Fig. 22). This kind of strong blocking effect was not clearly detected in the field observations by constant-pressure balloons. However, similarly strong streamline deviations are obtained from the computer results by Marwitz et al., (20).

5.2 Diffusion Properties

The vertical and horizontal dispersion widths of the Krypton-85 plume in the wind tunnel at several downstream points are given in Table 1 for neutral and stably stratified airflow cases. The lateral plume width is defined as the distance from the plume axis to the point where the concentration decreases to 10 percent of the peak value. The vertical plume height is defined by the height where the concentration decreases to one-tenth of the ground level value. The vertical dispersion is quite strongly regulated by the stratification,

especially in the lee side. In the field experiment by Smith and Heffernan, the lateral plume width at 10 km downstream is reported to to reach 3 to 5 km. However, in their report, the definition of the plume width is not given and direct comparison is difficult. The non-dimensional concentration of Krypton-85 defined by $\frac{C\bar{U}h^2}{Q}$ is 0.35 in neutral airflow and 1.5 in stable cases, at 18 km downstream of the source number 6. In the field, the non-dimensional concentration varies from 0.03 to 0.12 at the peak of Elk Mountain. These values are smaller than the wind-tunnel values, however, they are in close agreement with values obtained for neutral flow in the laboratory.

Table 1. Dispersion width in Wind Tunnel
(source number 6)

	Neutral		Stable	
x km	Lateral km	Vertical km	Lateral km	Vertical km
5	1.3	0.57	---	---
10	2.8	0.95	3.0	0.77
15	5.0	1.20	3.7	1.15
20	5.8	2.10	7.5	0.78

VI. SUMMARY AND CONCLUSIONS

6.1 Summary of the Study

6.1.1 Airflow model and simulation in wind tunnel - The laboratory simulation of airflow and dispersion were investigated for both neutral and stably-stratified cases. For stably-stratified case, the wind tunnel velocity was selected at 20 cm/s and dry ice blocks were used in addition to cooling of plate floor by refrigeration. By means of atmospheric soundings, the planetary boundary-layer thickness was estimated to be nearly 1000 m and the mean potential temperature gradient was nearly 2^{o} K/km inside of boundary layer and 4^{o}K/km in the upper layer. This 2 layered atmosphere was considered typical in winter time in the vicinity of Elk Mountain and was approximately simulated in the wind tunnel. For dispersion simulation, Krypton-85 radio-active gas was used as the tracer and was released from the source located 16 km upstream of Elk Mountain. General airflow features were as follows:

(1) Thermally near-neutral airflow layer which is comparable to the planetary boundary layer in the atmosphere was reproduced in the wind tunnel. The thickness of this layer was nearly 10 cm and the temperature was nearly constant in this layer. In the upper layer, the thermal stratification was much stronger and the temperature gradient was nearly 1.0^{o} c/cm.

(2) The stably stratified airflow was investigated for a wind speed of 20 cm/s. In spite of the upstream devices such as

dam and dry ice, the airflow was quite steady and the only wake effects observed were due to the topographic model.

(3) The velocity profile was fairly difficult to control for the low velocity in this study. However, by selecting the freestream velocity carefully and placing a dam in the downstream side, a satisfactory profile was obtained.

(4) The dry ice blocks persisted for 8 hours, and for the first 6 hours, the airflow properties were fairly steady.

6.2 Comparisons of the Model and Prototype Airflow and Dispersion

As the airflow similarity parameters, a bulk Richardson number and Froude number based on the height of the inversion base were considered. The airflow properties are as follows:

(1) The bulk Richardson number showed good agreement with the prototype in surface near neutral layer up to 10 cm from the surface. However, in the upper layer, the wind tunnel Richardson number was twice as large as the value in prototype.

(2) Froude number defined by the height of near neutral air layer was 0.20 in laboratory and was in good agreement with a value of 0.15 in prototype.

(3) The velocity profile in the wind tunnel was nearly flat with height and the surface drag effect was regulated in only the bottom part of the near neutral layer. This might have occurred because of near laminar character of the wind tunnel airflow.

(4) The blocking effect of the mountain was found to be exaggerated by the density stratification in the wind tunnel, although constant-pressure balloon trackings in the field did not show it clearly.

(5) The dispersion properties are fairly well simulated in the wind tunnel. At 10 km downwind from the source, the lateral dispersion width was 3 km in stably stratified cases. This value is nearly comparable to 1.0 to 3.7 km in prototype, although there is some ambiguity in the definition of plume width in the field. The lateral dispersion width in neutral airflow was nearly equal to the stable case. In the prototype the dispersion width was reported to increase with an increase of stability. This feature was explained by the increase of blocking effects caused by density stratification (3).

(6) Vertical dispersion was shown to be influenced by existing temperature inversions. Especially it was clear in the lee of the mountain where the vertical dispersion was smaller than the value at the ridge. By Auer et al., (3) the vertical dispersion in Elk Mountain was reported lower than 450 m at 10 km downstream of the source. However, the measurements were limited in number and the soundings were done for a strong superadiabatic condition.

6.3 Feasibility of the Shallow Water Analogy in Wind Tunnel

The computer simulation of airflow over Elk Mountain by shallow water equations was done by Marwitz et al., (20). Although the

Froude number in their work was different from this wind-tunnel study, we compared the wind tunnel results with their results.

(1) The occurrence of a hydraulic jump in the lee of the mountain was verified in the wind tunnel. However, the wind velocity at the lee slope was not as high in the wind tunnel as suggested by the computer results. Limited soundings in the field also seemed to show the highest wind velocity at the ridge. The wind-tunnel results seemed to be closer to the field results. In the wind-tunnel the highest horizontal velocity was found at the ridge and it increased to 170 percent of the upstream value.

(2) The height distribution of the temperature inversion surface in the wind tunnel showed reasonable agreement with field results and also with computer results. The highest point was coincident with the highest topography and the lowest occurred in the lee of the mountain. However, the height change in the wind tunnel was not so great as in the computer results.

(3) The vertical stream surface was not clearly definable in stably stratified cases in the wind tunnel because of strong mixing in the surface layer. However, the estimated mean stream surface by dispersion measurement showed reasonable agreement with computer results.

6.4 Conclusions

Stably-stratified airflow over an isolated mountain has been shown to be simulated fairly well in the wind tunnel. The wind tunnel

results agree qualitatively with the field observation and also with the theoretical results by shallow-water analogy.

The hydraulic jump and over-all flow pattern were reproduced well in the wind tunnel by considering a Froude number and bulk Richardson number similarity. However, the small structure of airflow such as velocity profiles or temperature profiles are quite difficult to simulate by this similarity concept, since the above similarity requires very low wind velocities and then the airflow becomes nearly laminar and the effect of the surface roughness decreases.

Accordingly, if we are concerned about the fine structure of the airflow both Richardson and Reynolds number similarity should be achieved. However, if the airflow scale is fairly large and there exists a density discontinuity surface, Froude number similarity in addition to geometrical similarity is sufficient to insure similarity of the large scale air motions. Since in this simulation study of stably stratified airflow mean large-scale flow properties may have been simulated well, advective transport processes have been simulated with equal accuracy.

Horizontal dispersion in the model compared well with prototype data, although some ambiguity exists in the field results. Only limited data on vertical dispersion were available from the Elk Mountain field study and Auer et al., (30) stated that the vertical dispersion was limited to a height below 450 m for a strong superadiabatic atmosphere. This height is less than that found for the wind tunnel dispersion. Then the vertical dispersion should be similar to that for the prototype as long as the inversion height is similar over laboratory model and prototype, and the distance downwind from the source is sufficient

for dispersion to take place throughout the mixing layer. Therefore, as long as the selected mean airflow properties over Elk Mountain are typical for winter time, the wind-tunnel transport dispersion characteristics are expected to simulate the mean transport-dispersion properties in the prototype.

BIBLIOGRAPHY

BIBLIOGRAPHY

1. Abe, M., 1941, Mountain cloud, their forms and connected air currents: Bull. Central Met. Obs., part 2, Japan 7-3.

2. Arya, S. P. S. and Plate, E. J., 1969, Modeling of the stably stratified atmospheric boundary layer: Jour. Atmos. Sci., 26, pp. 656.

3. Auer, A. H., Jr., Veal, D. L. and Marwitz, J. D., 1970, Some observations of silver iodide plumes within the Elk Mountain Water Resources Observatory: Jour. Weather Modification, 2-2, pp. 122.

4. Batchelor, G. K., 1953, The conditions for dynamical similarity of motions of a frictionless perfect gas atmosphere: Quart. J. R. Met. Soc., 79, pp. 224.

5. Blackadar, A. K., 1962, The vertical distribution of wind and turbulent exchange in a neutral atmosphere: Jour. Geophys. Res., 67, pp. 3095.

6. Cermak, J. E. and Peterka, J., 1966, Simulation of wind fields over Point Arguello, California, by wind tunnel flow over a topographic model: Tech. Rept. CER-65-JEC-JAP64, Colorado State University.

7. Cermak, J. E., Grant, L. O. and Orgill, M. M., 1969, Research and development technique for estimating airflow and diffusion parameters in connection with the Atmospheric Water Resources program: Tech. Rept. 14-06-D-6455, Colorado State University.

8. Chaudhry, F. H. and Meroney, R. N., 1969, Turbulent diffusion in a stably stratified shear layer: Tech. Rept. C-0423-5, Dept. of Civil Engr., Colorado State University.

9. Hanna, S. R., 1968, A method of estimating vertical eddy transport in the planetary boundary layer using characteristics of vertical velocity spectrum: Jour. Atmos. Sci., 25, pp. 1026.

10. Hanna, S. R., 1969, The thickness of the planetary boundary layer: Atmos. Envir., 3, pp. 519.

11. Houghton, D. D., and Kasahara, A., 1968, Nonlinear shallow fluid flow over an isolated ridge: Comm. Pure and Applied Math., 21, pp. 1.

12. Houghton, D. D., 1970, Numerical simulation of strong mountain wind: Proceedings of the 1970 Summer Computer Simulation Conference, pp. 1001.

BIBLIOGRAPHY - (Continued)

13. Kao, T. W., 1965, The phenomenon of blocking in stratified flows: Jour. Geophys. Res. 70, pp. 815.

14. Laikhtman, D. L., 1961, Physics of the boundary layer of the atmosphere: Translated by the Israel program for scientific translation, Jerusalem.

15. Lavoie, R. L., 1968, A meso-scale numerical model and lake effect storm: Ph.D. dissertation, Penn. State University.

16. Lettau, H. H., and Davidson, B., eds., 1957, Exploring the atmosphere's first mile: Pergamon Press, New York.

17. Lettau, H. H., 1962, Theoretical wind spirals in the boundary layer of a barotropic atmosphere: Beit, Phys. Atmos. 35, pp. 195.

18. Long, R. R., 1953, Some aspects of the flow of stratified fluids: Tellus, 5-1, pp. 42.

19. Long, R. R., 1955, Some aspects of the flow of stratified fluids: Tellus, 7, pp. 341.

20. Marwitz, J. D., Veal, D. L., Auer, A. H., Jr., and Middleton, J. R., 1969, Prediction and verification of the airflow over a three-dimensional mountain: Tech. Rept. 60, Natural Resources Res., Institute, University of Wyoming.

21. Oobayashi, T., 1970, A numerical study of two-dimensional airflow over an isolated mountain: Jour. Meteo. Society, Japan, 48-2, pp. 118.

22. Orgill, M. M., 1971, Laboratory simulation and field estimates of atmospheric transport-dispersion over mountains: Ph.D. dissertation, College of Engr., Colorado State University.

23. Panofsky, H. A., and Lumley, J. L., 1964, The structure of atmospheric turbulence: Interscience.

24. Queney, P., et al., 1960, The airflow over mountains: World Met. Organ. Tech. Note 34.

25. Rossby, C. G. and Montgomery, R. B., 1935, The layer of frictional influence in wind and ocean currents: Paper Phys. Oceanog. Met. 3-3, pp. 101.

26. Scorer, R. S., 1949, Theory of waves in the lee of mountains: Quart. J. R. Met. Soc. 75, pp. 41.

BIBLIOGRAPHY - (Continued)

27. Scorer, R. S., 1953, Theory of airflow over mountain 2 - The flow over a ridge: Quart. J. R. Met. Soc. 79, pp. 70.

28. Scorer, R. S., 1967, Causes and consequences of standing waves: Proceedings of the Symp. on Mountain Meteorology, Dept., Colorado State University, pp. 75.

29. Sheppard, P. A., 1956, Airflow over mountains, shorter contribution: Quart. J. R. Met. Soc. 82, pp. 226.

30. Smith, E. J. and Heffernan, K. J., 1956, The decay of the ice-nucleating properties of silver iodide released for a mountain top: Quart. J. R. Met. Soc. 82, pp. 182.

31. Tag, P. M. and Spelman, M. J., 1969, Atmospheric modification by surface influences: Rept. 15, Dept. Met., Penn. State University.

32. Wallington, C. E., 1958, A numerical study of the topographical factor in lee wave amplitude: Quart. J. R. Met. Soc. 84, pp. 428.

33. Willis, P. T., 1968, Diffusion in an orographic environment: Paper presented at Third Sky Water Conference.

APPENDICES

APPENDIX I

TOPOGRAPHIC MODEL AND WIND TUNNEL

APPENDIX I

TOPOGRAPHIC MODEL AND WIND TUNNEL

A topographic model was constructed of ¼ inch thick polystyrene bead board cut along contour lines of an enlarged topographic map. Roma Plasticene was used to smooth the model and sand particles were scattered and fixed on the surface by paint to simulate the roughness such as vegetation or large rocks. The scale of the model is equal in the vertical and horizontal and was chosen to be 1:9600. The optimum operational wind direction was decided as 250^{o} or west-southwest by inspection of meteorological data for the area. The lowest or reference elevation in this area is 6800 feet and the highest is Elk Mountain of 11,156 feet. The maximum height of the model is 13.8 cm and the dimensions are 1.8 x 3.7 m. Elk Mountain is an isolated hill, but hills to the north and south complicate the topography. The windward slope of the mountain rises gradually from a sagebrush plain while the lee-ward slope descends steeply from 11,000 feet to 8000 feet plain within 3 km.

The model experiment was performed in the meteorological wind tunnel in the Fluid Dynamics and Diffusion Laboratory at Colorado State University. The wind tunnel is a recirculating type with a test section of dimensions 29 m long and 2 m by 2 m in cross section. The downstream half of the test-section floor can be either heated electrically or cooled by cold brine through a system of pipes installed in the floor. The ambient air temperature in the wind tunnel is also controllable by a system of heating or cooling coils in the return section. Since in the simulation of stably stratified atmosphere strong temperature gradient

was required the floor plates were cooled to $0^{o}C$, ambient air was heated to $32^{o}C$ and dry ice blocks were also located at the upstream of the test section. Although Froude number similarity requires low velocity of nearly 20 cm/s, the minimum controllable wind velocity is 1 m/s, so that two screens with 16% open area were set at both ends of the test section to decrease the wind velocity to the required value.

APPENDIX II

EXPERIMENTAL EQUIPMENT AND PROCEDURE FOR NEUTRAL AIRFLOW

APPENDIX II

EXPERIMENTAL EQUIPMENT AND PROCEDURE FOR NEUTRAL AIRFLOW

Flow Field Measurements

Stream-lines, wind velocity and dispersion properties were investigated for neutral airflow. The free stream velocity was selected to be 9 m/s for experimental convenience. To make the velocity profile similar to the field, L-shaped aluminium rods of 2.5 cm high were located on the floor upstream of the model. By this roughness the wind velocity was reduced near the surface and made similar to the field profile. The wind velocity was measured by pitot tube and diaphragm type pressure transducer (Transonic Pressure Meter Type 120). The electric signals from the pressure transducer and the potentiometer for vertical position of the probe were supplied to a X-Y plotter. The velocity profiles were recorded automatically by lifting the pitot tube continuously from model surface to the top of the boundary layer. The pitot tube was moved slowly as not to deform the true velocity profile.

The streamlines were determined from the wind direction measurements by miniature bi-directional vanes of 2 cm length. These vanes were set on the model at height of 2 cm and photographed from the top of the wind tunnel. To draw the stream lines, the photographs were enlarged to the same scale as the geographic map and vane directions were transferred to the map.

Dispersion Measurements

The diffusion measurements were made using radioactive Krypton-85 gas as the tracer. The tracer gas was released from source point 6,

which is located west south-west of Elk Mountain. The distance from the source to the mountain peak is about 17.5 km and the elevation of the source site is about 7000 feet. The tracer gas was released continuously for 3 or 4 minutes and the gas mixture was sampled by 3mm dia. steel pipes and introduced to the Geiger-Mueller tubes. The radioactivity level of the sampled gas was measured by an electronic counter. This device was first developed by Chaudhry (8) and described precisely in his report.

APPENDIX III

EXPERIMENT FOR STABLY-STRATIFIED AIRFLOW

APPENDIX III

EXPERIMENT FOR STABLY-STRATIFIED AIRFLOW

Airflow Production in Wind Tunnel

The schematic expression of the experiment is shown in Fig. 2. As stated before, the ambient air temperature and the floor temperature were controlled to 32°C and 0°C respectively. Since the thickness and stability of the stratified airflow produced by the installed facilities were not sufficiently similar to the prototype, about 500 lbs of dry ice blocks were located upstream of the model. The dry ice blocks set just downstream of a dam of 50 cm height which prevented the gravity current of cold air to move upstream. The distance between the dam and the scale model was taken to be 10 m to decrease the turbulence produced by the dam and dry ice. Seven I-shaped aluminum rods about 10 cm high and 1.8 m long were also placed on the cooled plate floor parallel to the flow to increase the cooling efficiency and to attenuate large scale turbulence. A dam 25 cm high with multiple holes was also placed at the downstream of the model to reduce the high wind velocity near the model surface caused by density stratification.

The dry ice blocks were brought into the wind tunnel after the temperature of airflow reached steady state. They lasted nearly 8 hours, but a one-hour period was required for the airflow to become steady. The airflow velocity was selected to be 20 cm/s to give Froude number similarity.

Velocity Measurement in Stably-Stratified Airflow

For the velocity measurement, the smoke-wire equipment was used. In the Point Arguello model study, Cermak and Peterka used constant-temperature hot-wire anemometer calibrated for low velocity. However, in this study the wind velocity was too low and temperature difference was too large for hot-wire sensing. The precise description of the smoke-wire system is given in the report by Orgill (22). The outline of the system operation is as follows:

> By vaporizing model train smoke oil supplied on a vertically supported tungsten wire of 38μ diameter with an instantaneous electric current, a vertical smoke line is produced in the wind tunnel. The picture of the smoke is taken in less than one second time delay by a camera combined with a strobo-flash.
>
> The mean velocity profile was determined by the distance of the line smoke traveled from its original position and the delay time. Since this is a Lagrangian method, and individual smoke picture may not indicate the usual Eulerian mean profile. Two or three pictures were taken for each measuring point and the mean profile was obtained as the average of them. The delay time was set at 500 milli-seconds. The smoke pictures were very clear and did not show dispersion of the smoke except in the neutral stability layer near the surface.

Temperature Measurement

The vertical temperature profiles were measured by fifteen thermocouples arranged vertically at 2 cm from each other. The small voltage signals from thermocouples were supplied and digitalized by a digital

voltmeter and then printed out by a digital printer. Since there was some amount of temperature fluctuation in the airflow, three readings were taken for each thermocouple and the average temperature was taken to be the mean of them. The temperature fluctuations were always less than one degree in centigrade.

Dispersion Measurement

The dispersion measurement was made in the same way as in the neutral case. However to decrease the buoyancy effect of the tracer caused by the temperature difference, Krypton-85 gas was introduced to cooling boxes containing dry ice before it was released from the source point. The intake velocity of the gas mixture into the sampling tubes was kept very low so as to not deform the true dispersion profile.

FIGURES

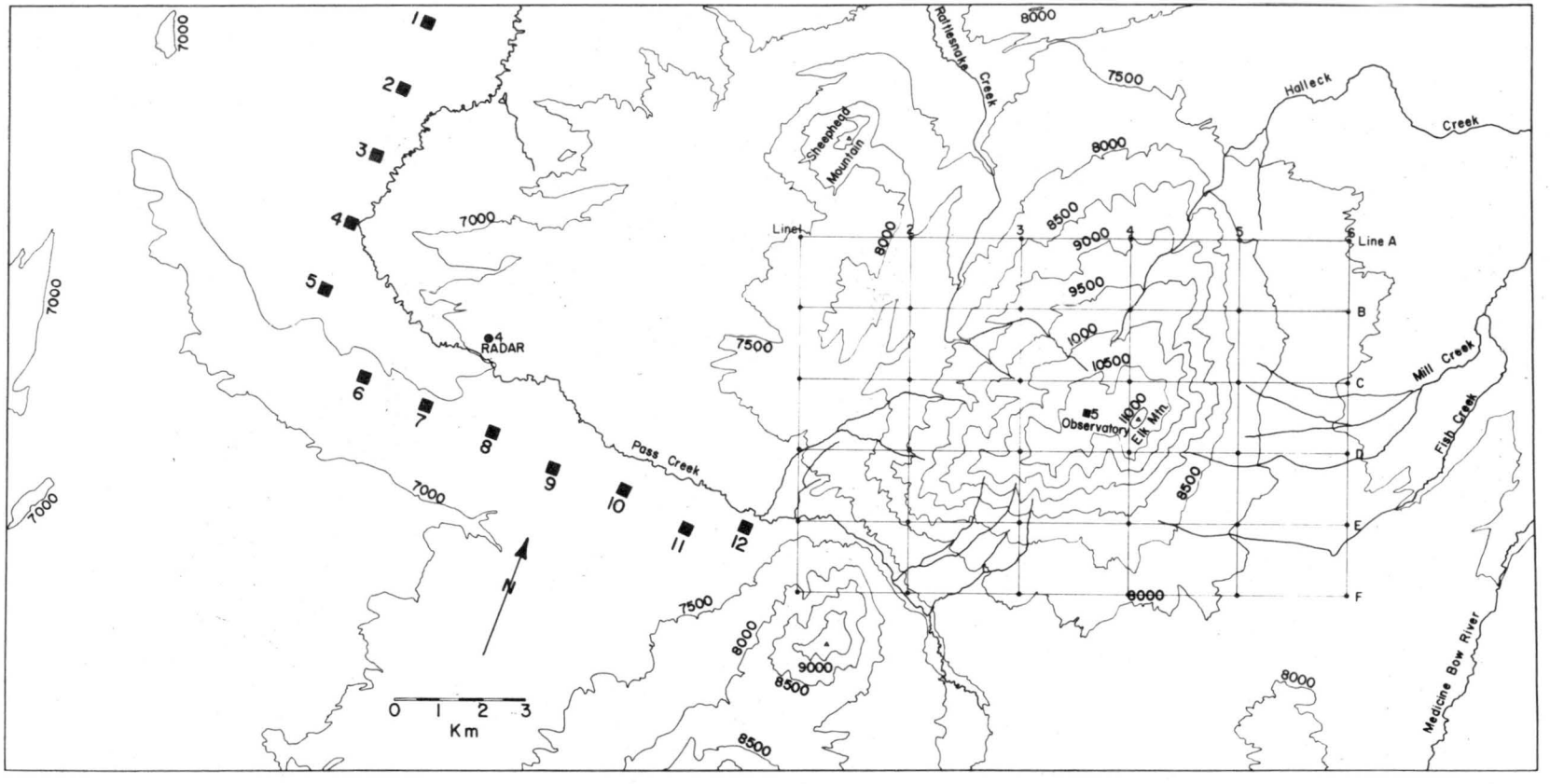

Fig. 1 Elk Mountain and surrounding topography modeled in wind tunnel, including measuring lines in laboratory experiment.

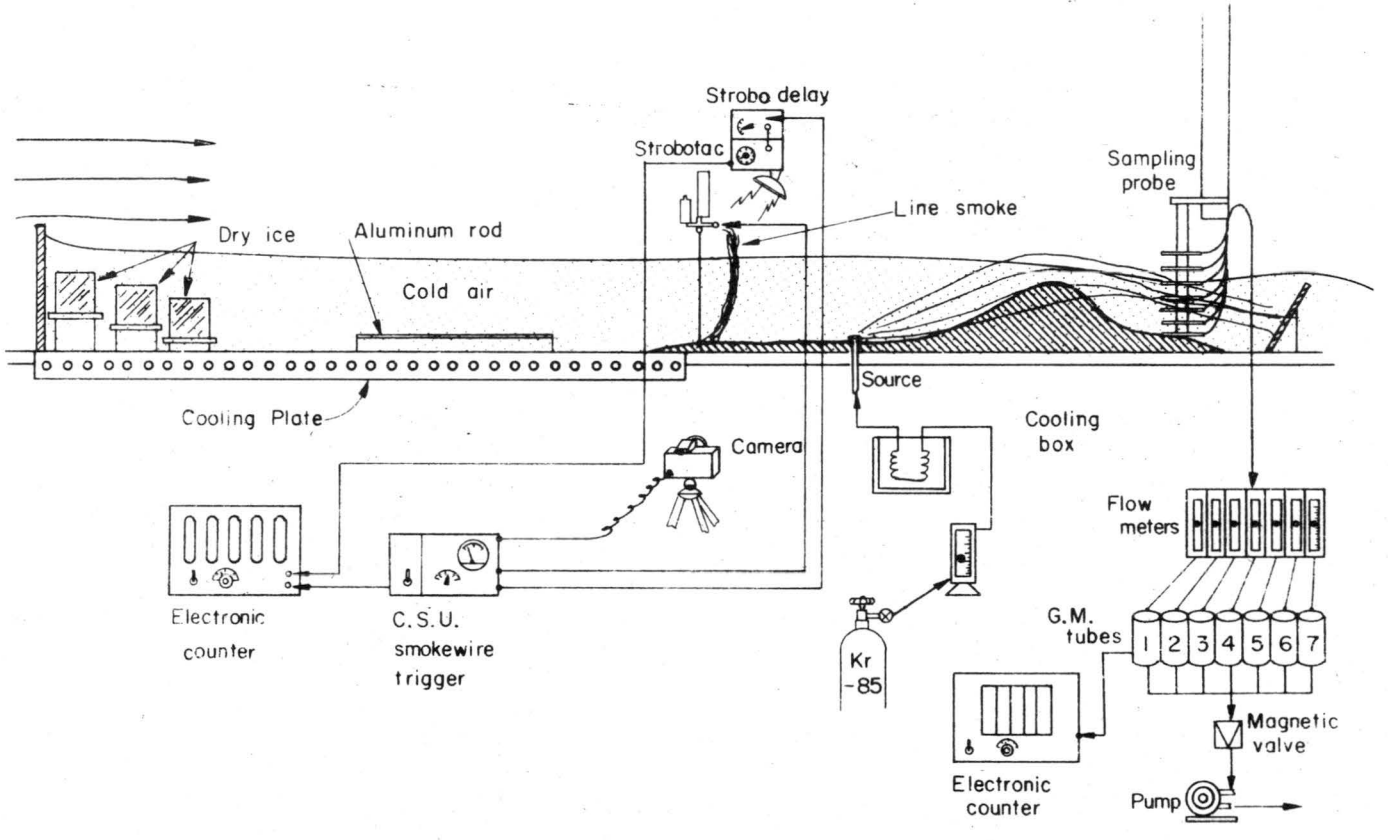

Fig. 2-1 Schematic figure of wind tunnel experiments.

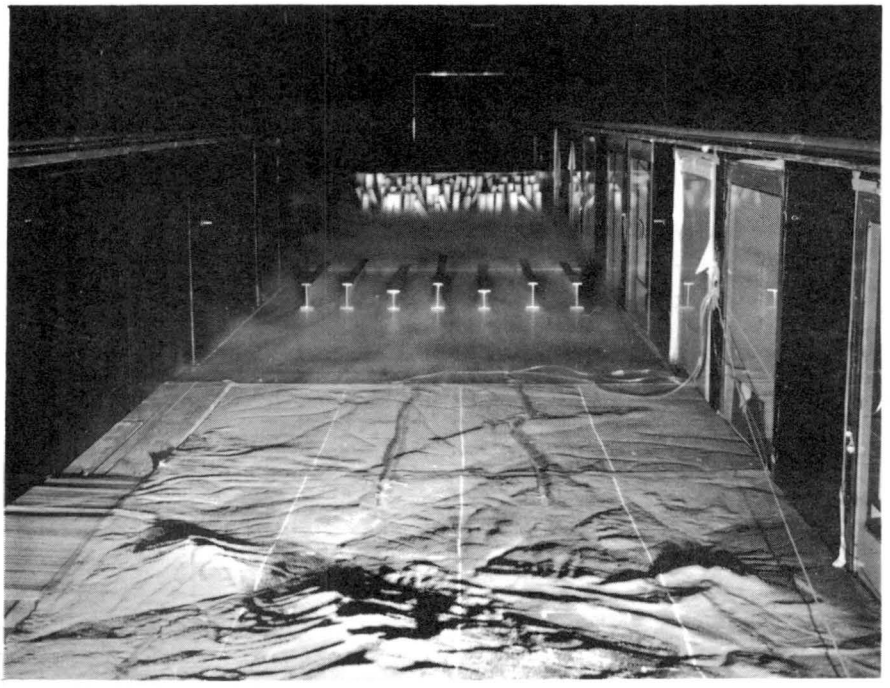

Fig. 2-2 Picture of wind tunnel and model set up.

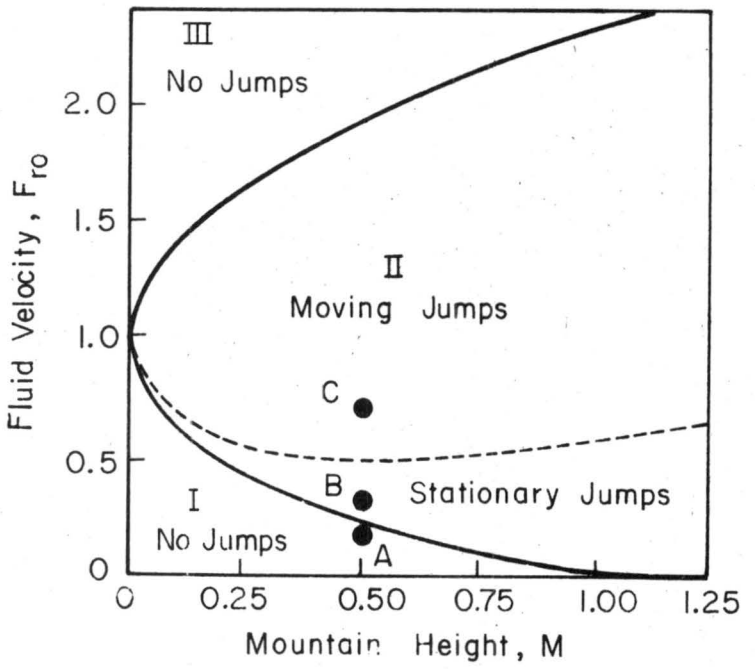

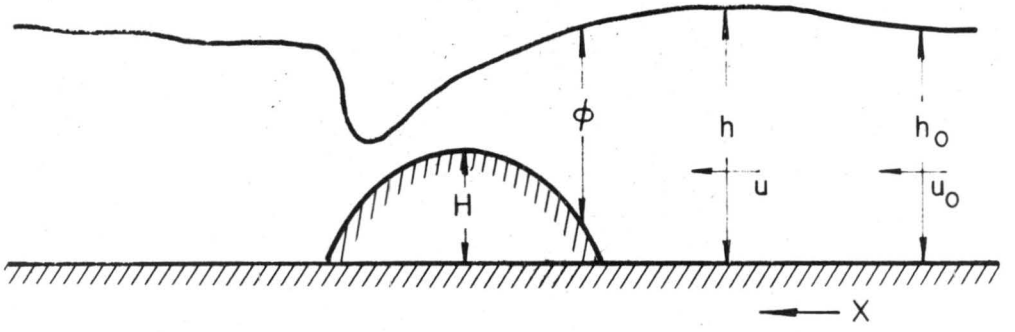

Fig. 3 Classification of flow conditions in shallow water equation system (from Houghton & Kasahara).

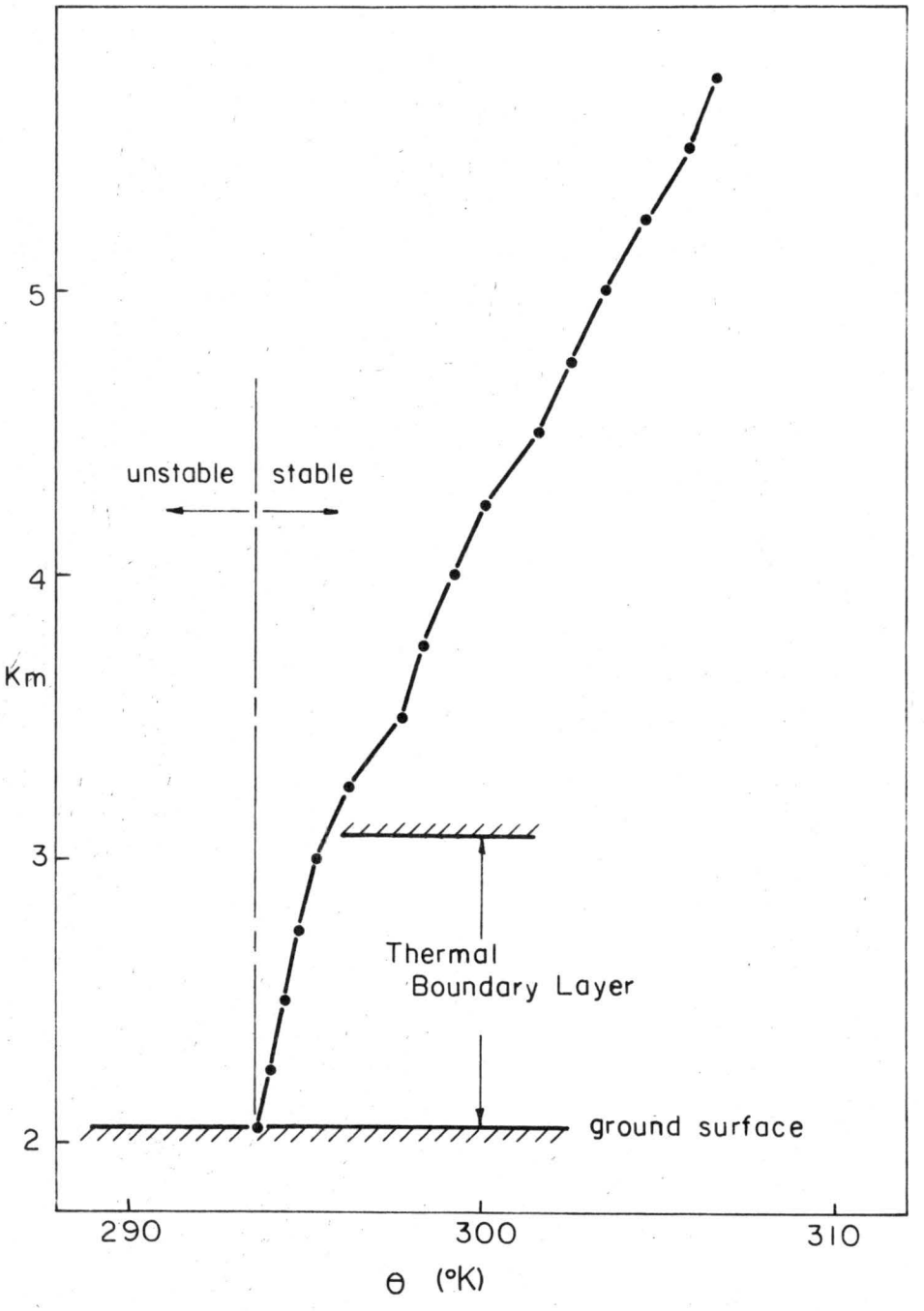

Fig. 4 Mean temperature profile at Elk Mountain radar site.

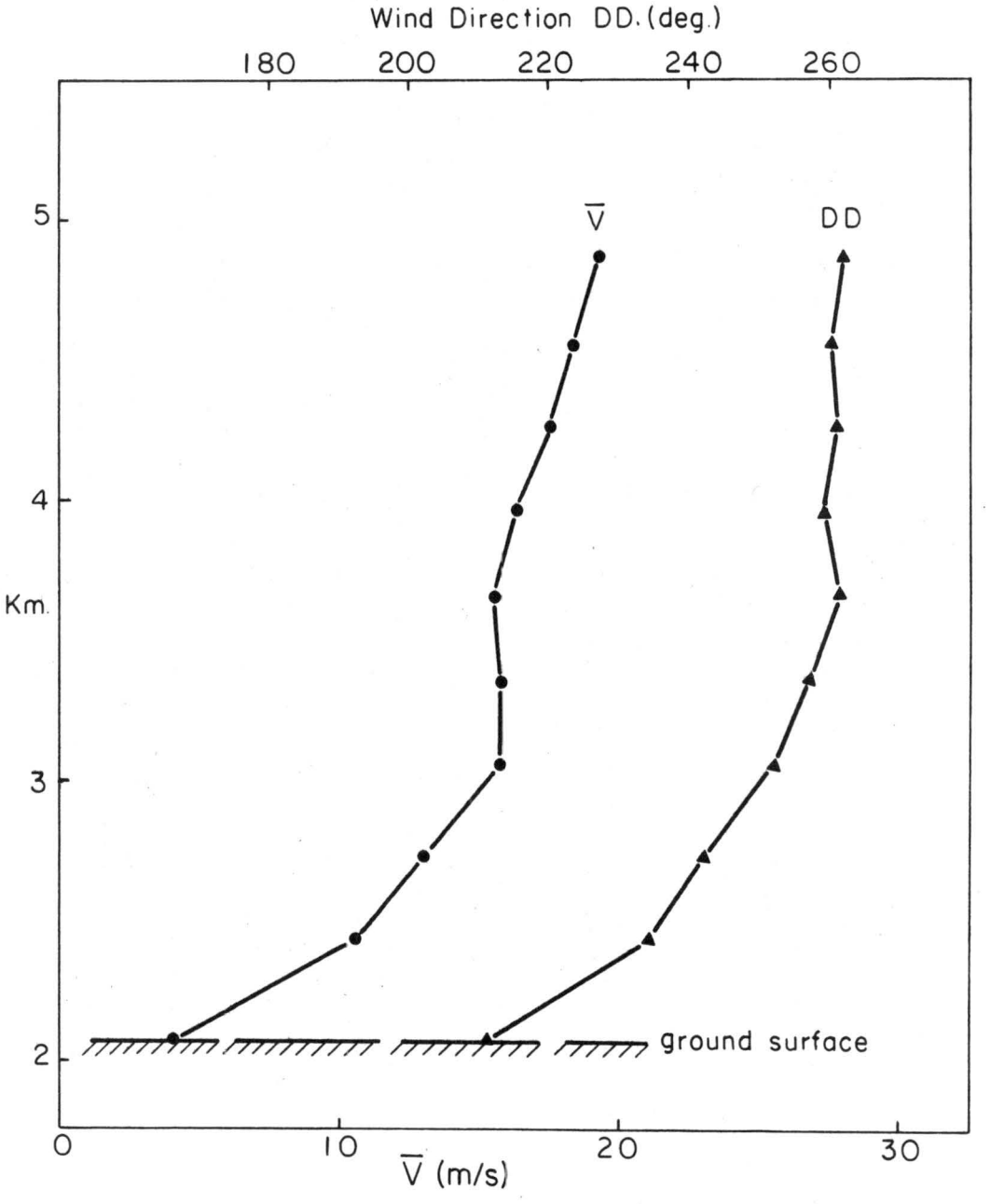

Fig. 5 Mean vertical profiles of wind velocity and wind direction at Elk Mountain radar site.

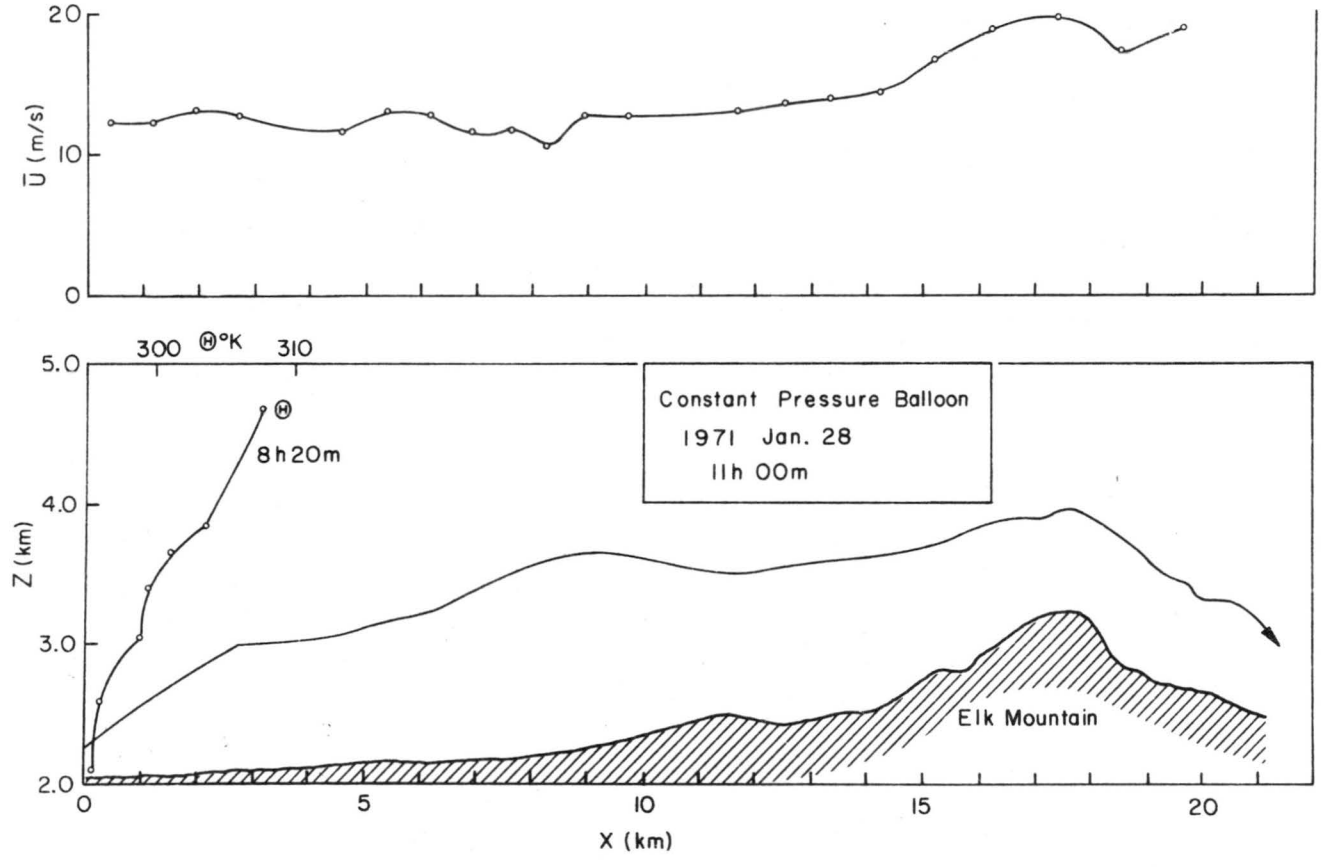

Fig. 6-1 Vertical trace of constant pressure balloon.

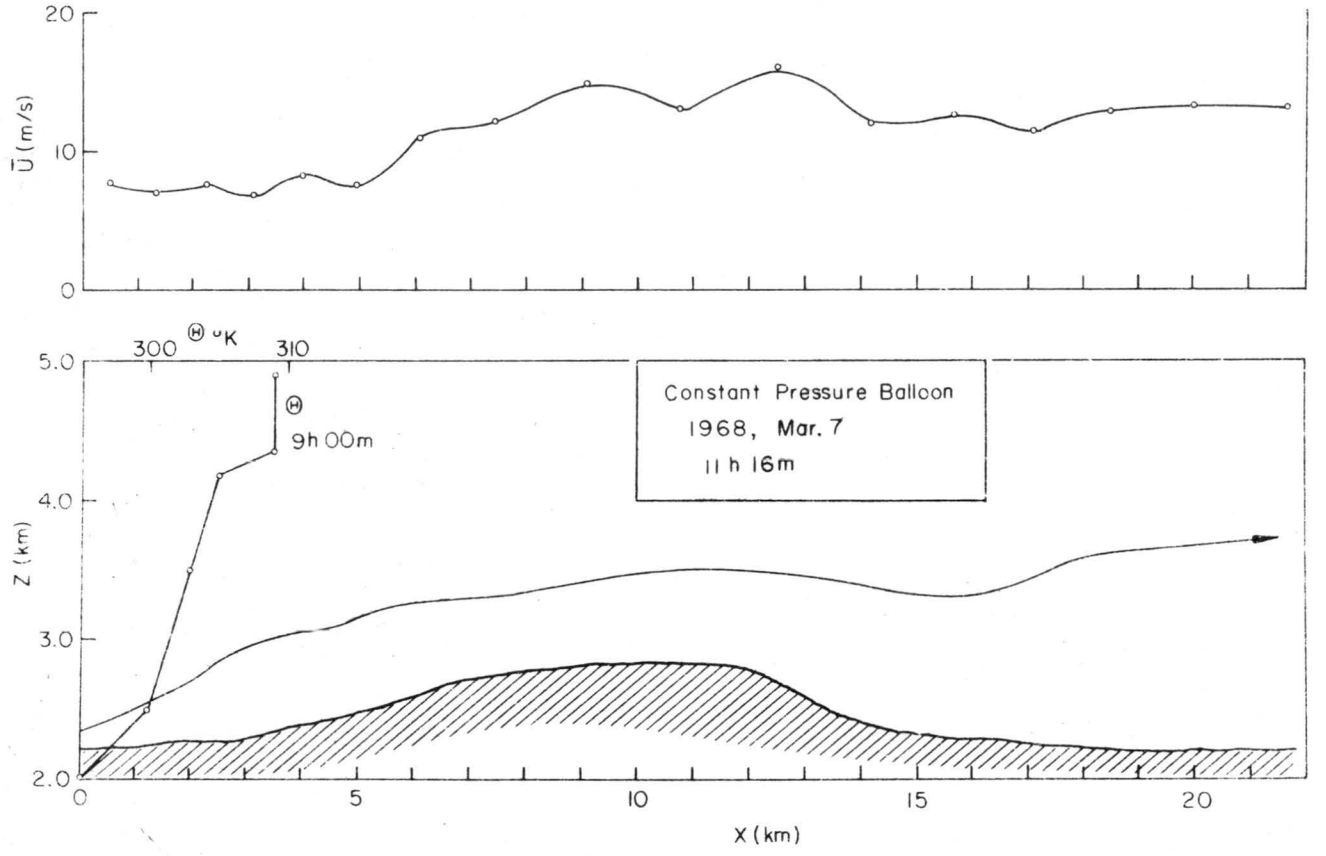

Fig. 6-2 Vertical trace of constant pressure balloon.

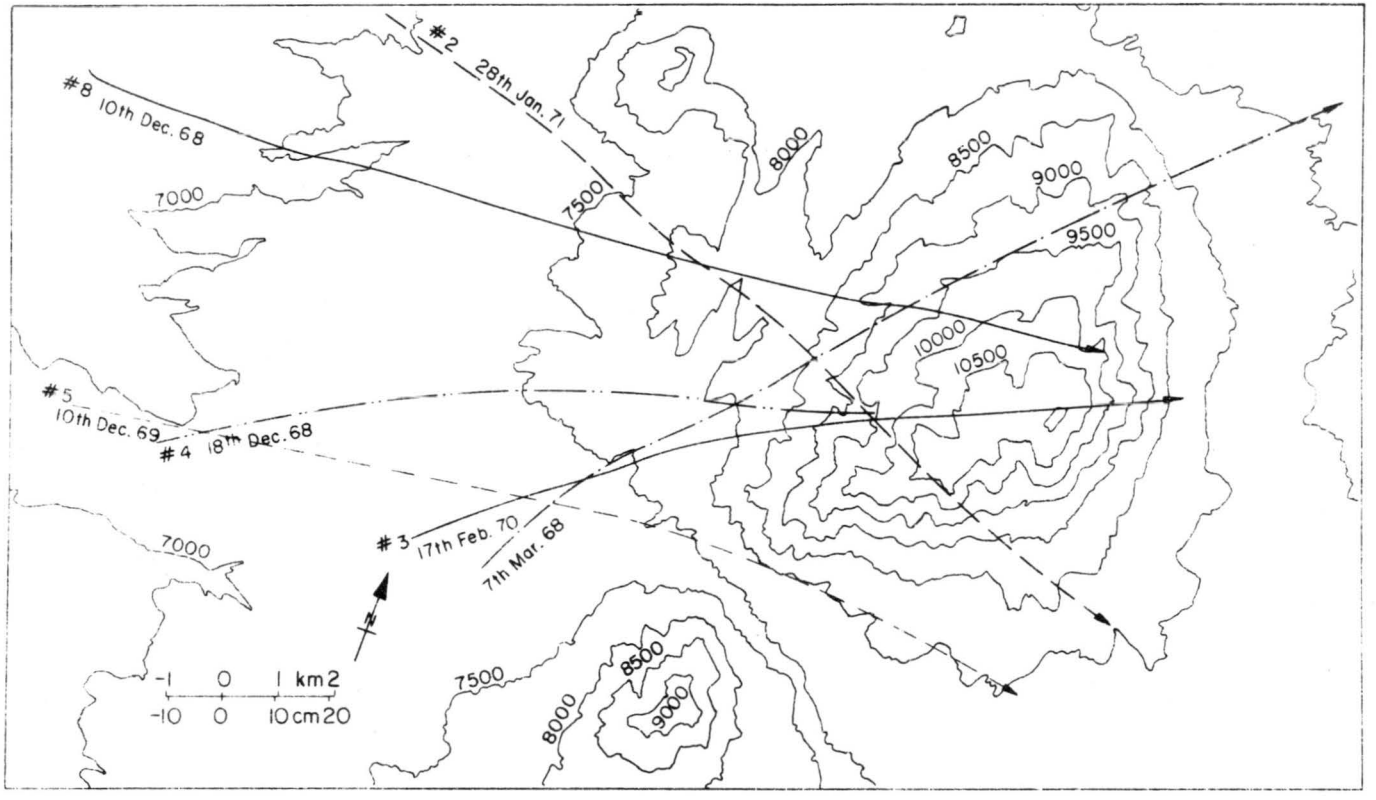

Fig. 7 Horizontal traces of constant pressure balloons.

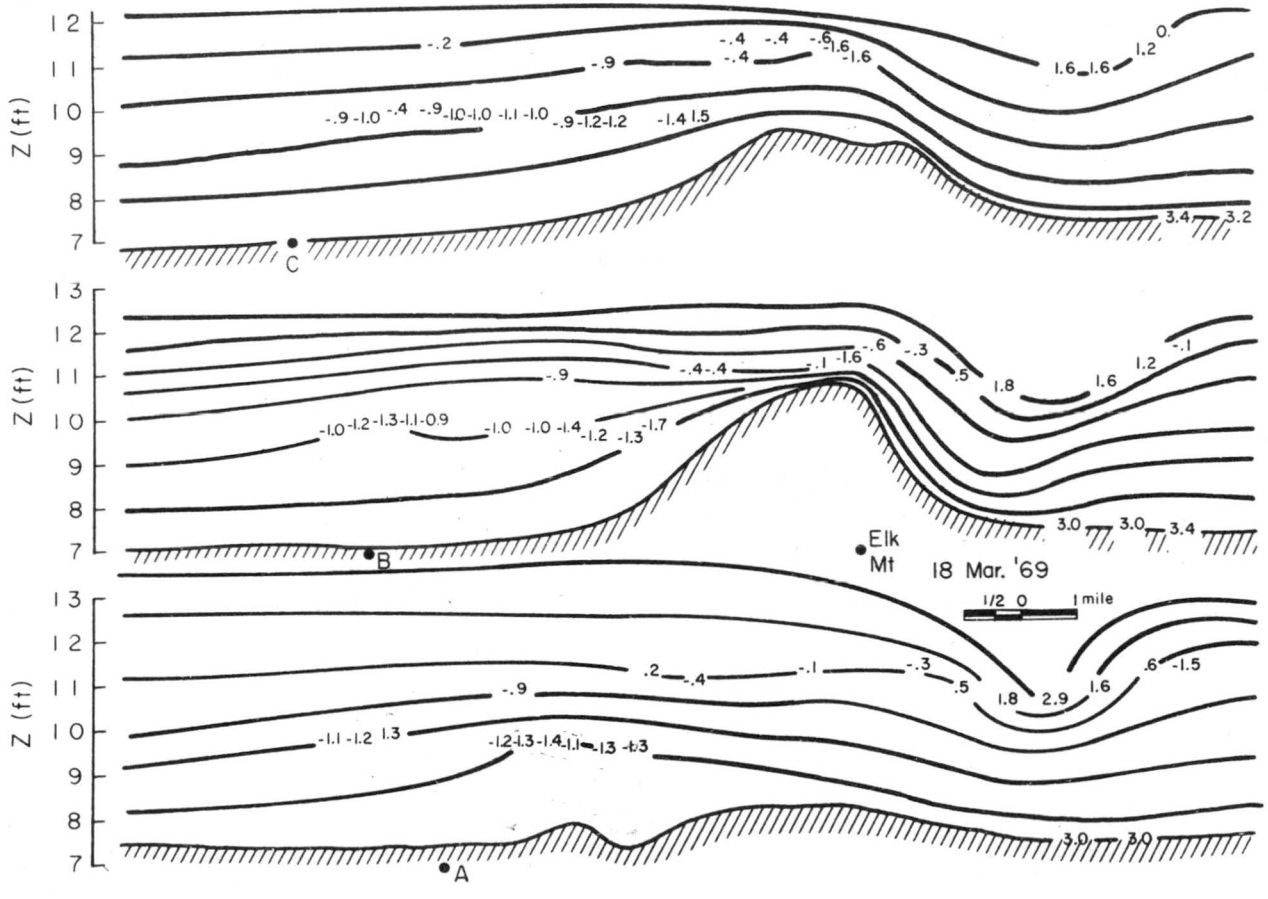

Fig. 8-1 Streamline distribution over Elk Mountain estimated from aircraft observations (from Marwitz et al.).

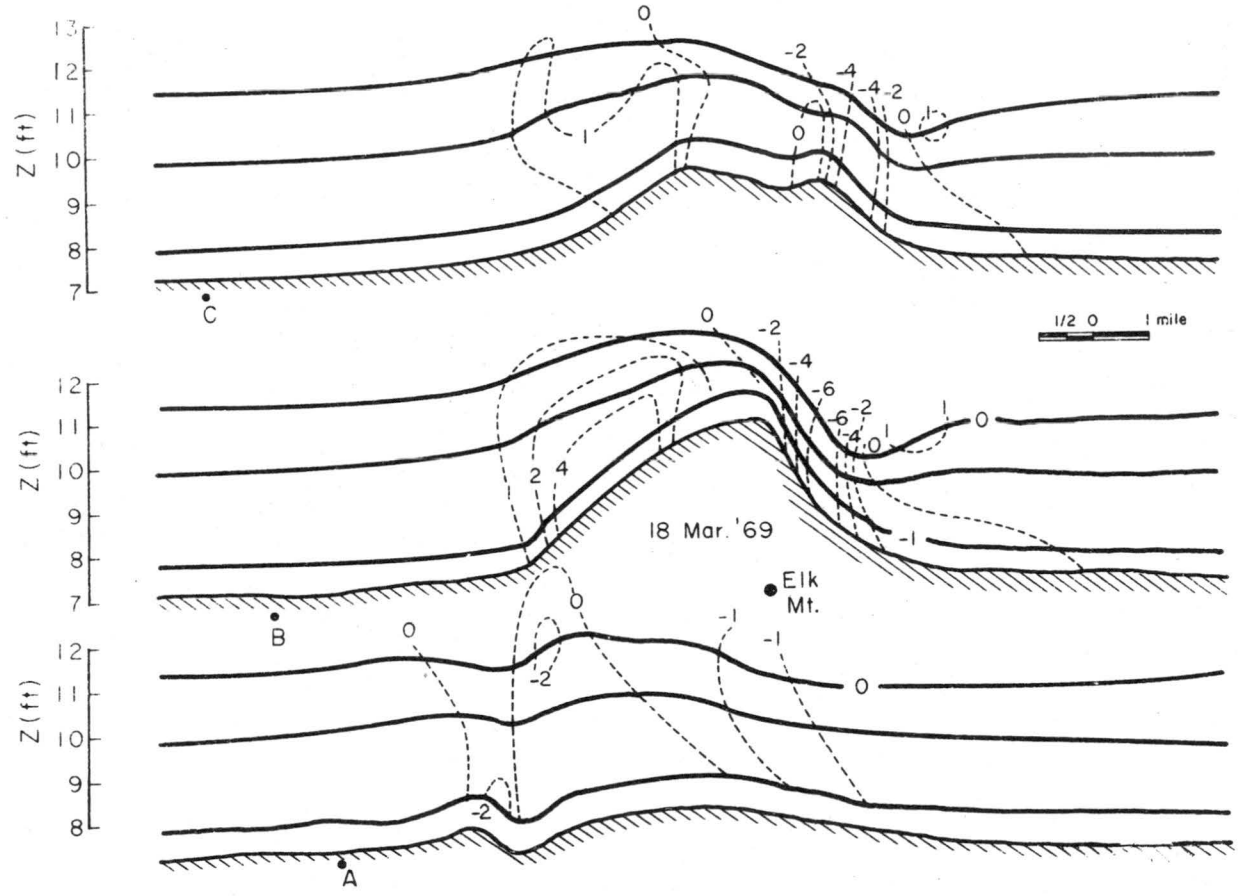

Fig. 8-2 Streamline distribution over Elk Mountain estimated by computer simulation based on shallow water model (from Marwitz et al.).

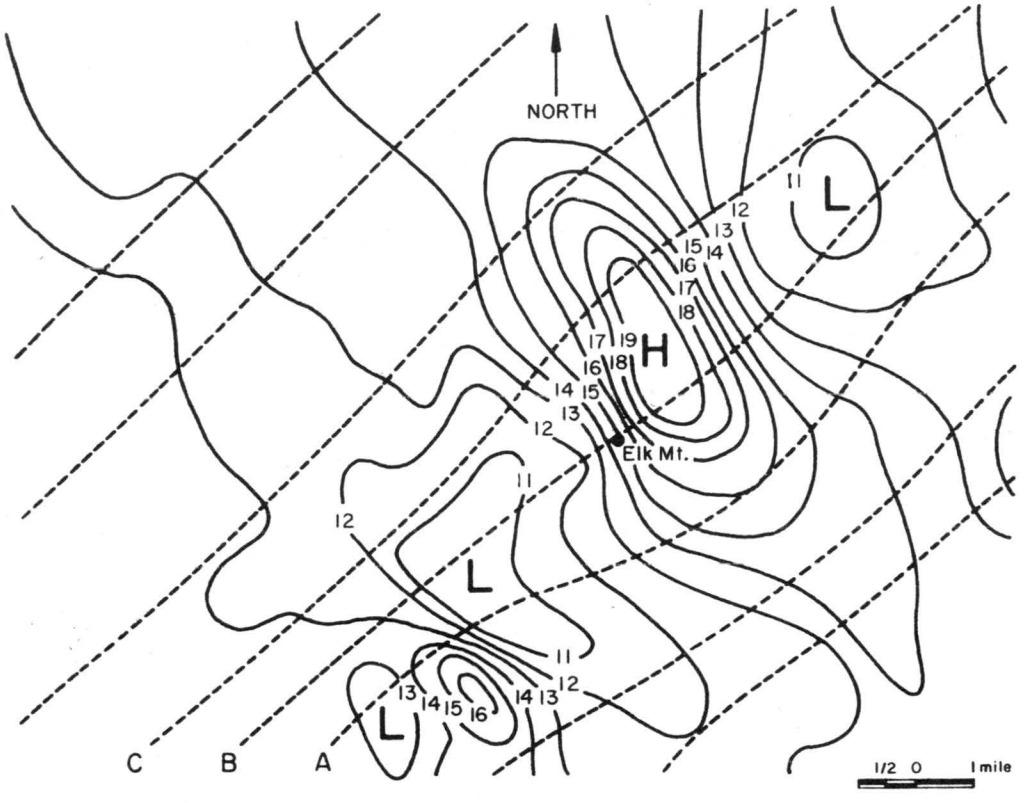

Fig. 9 Vertical stream surfaces and isotach field by computer model. (From Marwitz et al.). (Solid lines in meters per second).

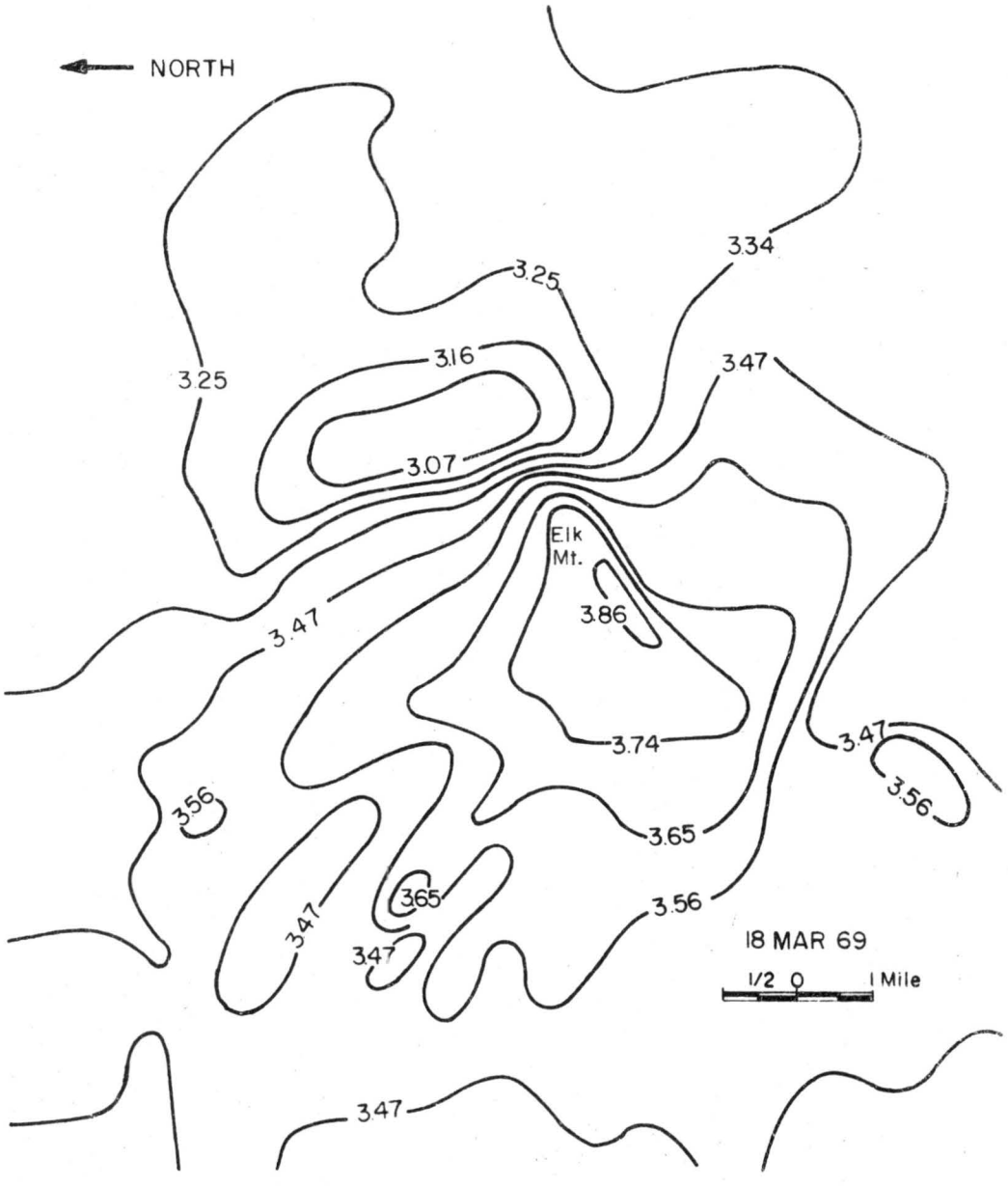

Fig. 10 Height of horizontal stream surface over Elk Mountain calculated by computer model. (Solid lines in Km -- from Marwitz et al.).

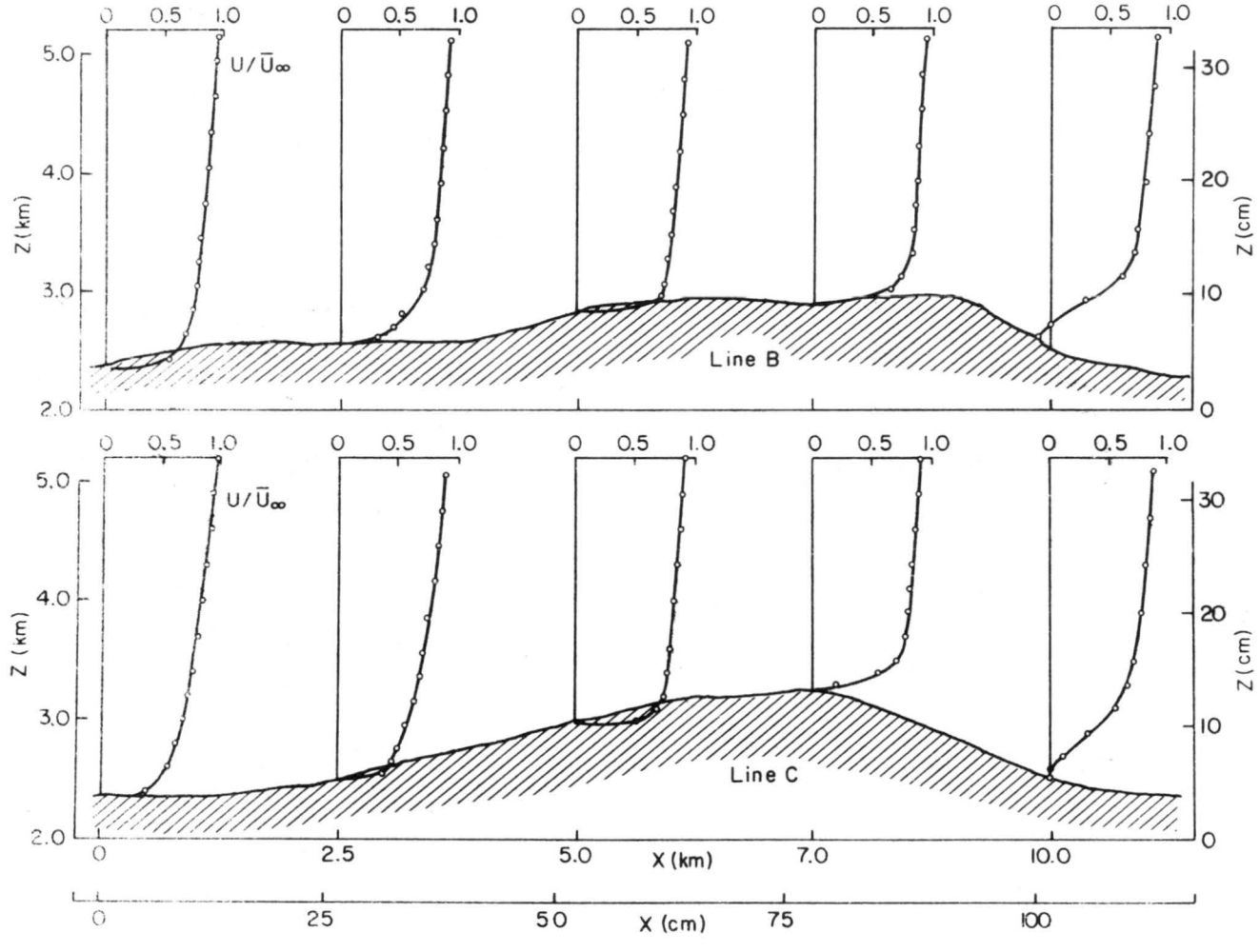

Fig. 11 Velocity profiles along lines B and C in neutral airflow over laboratory model.

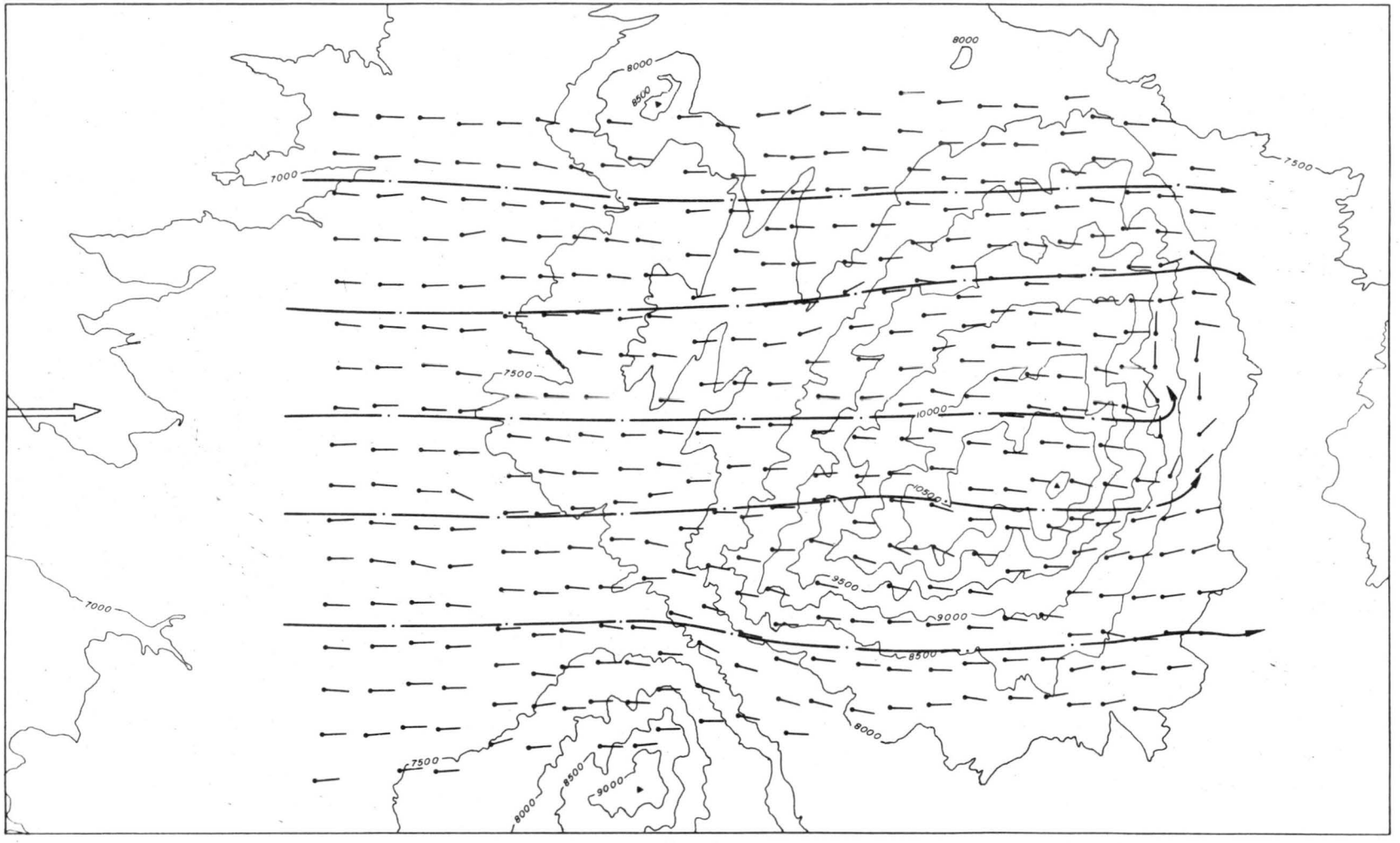

Fig. 12 Surface wind direction and estimated streamlines in neutral airflow over laboratory model.

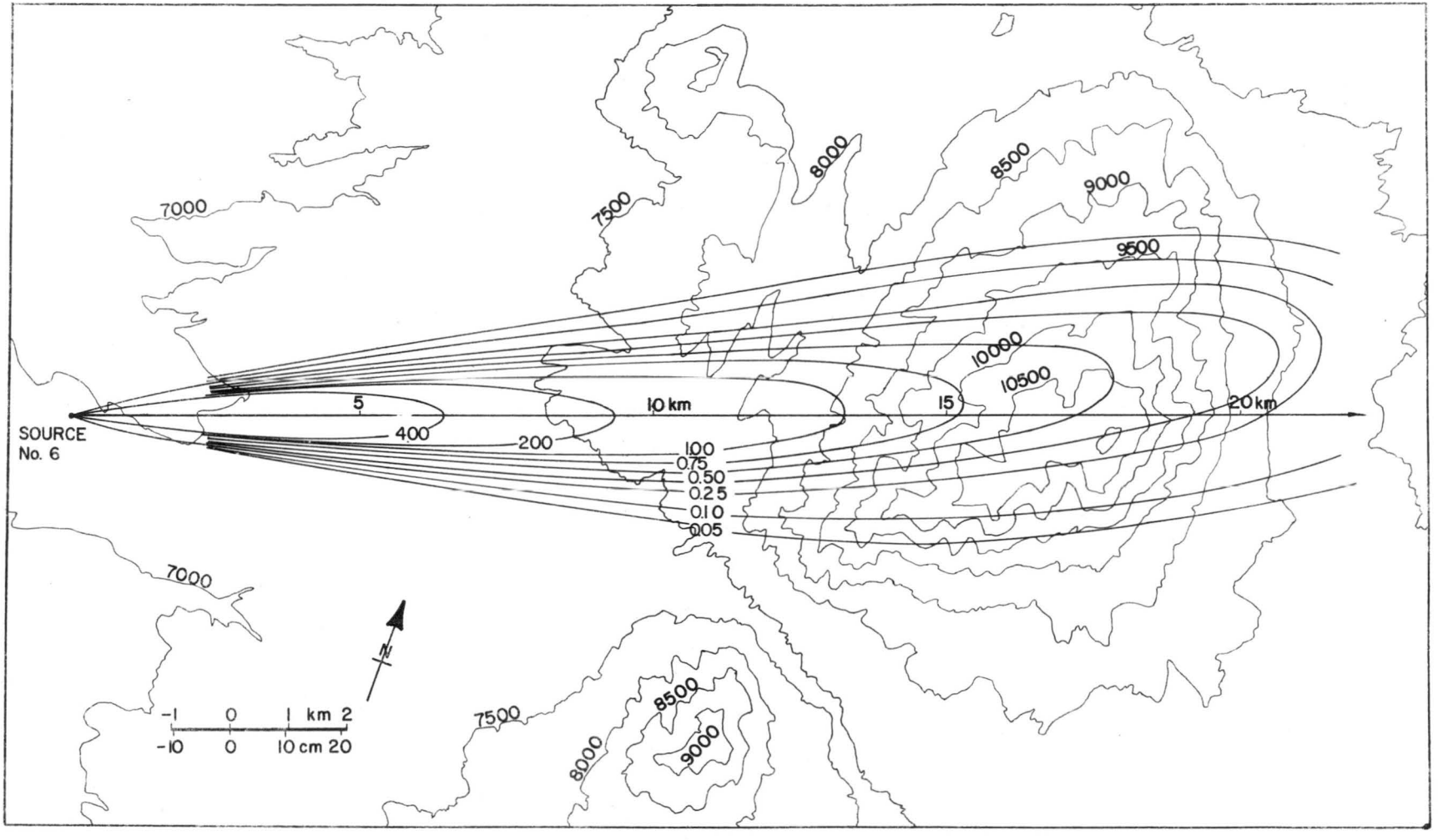

Fig. 13 Ground level contour lines of Krypton-85 in neutral airflows over laboratory model. Concentrations are non-dimensionalized by $\frac{C\bar{U}h^2}{Q}$.

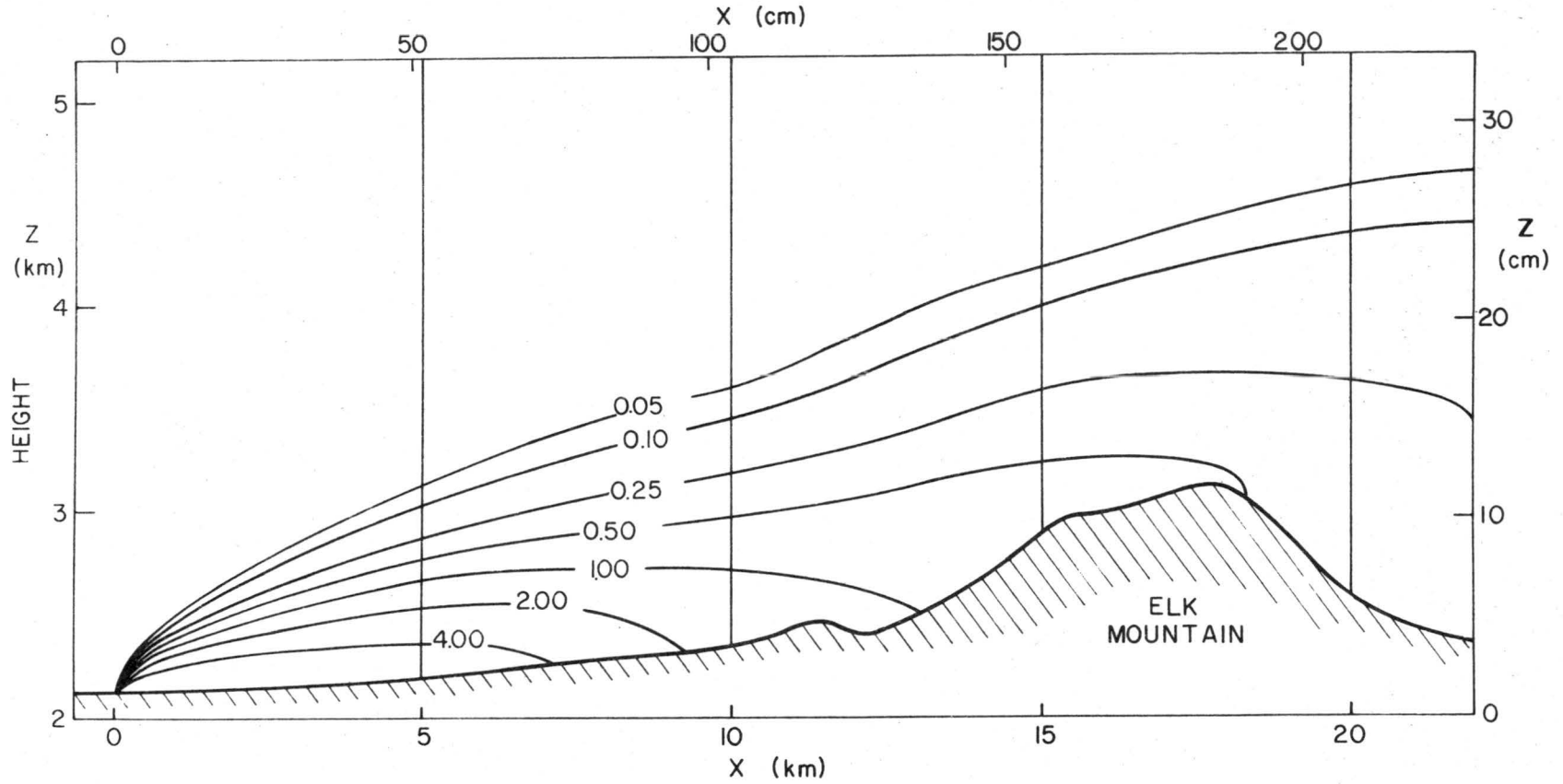

Fig. 14 Vertical contour lines distribution of Krypton-85 dispersion in neutral airflow. (Vertical plane through plume axis). Concentrations are non-dimensionalized by $\frac{C\bar{U}h^2}{Q}$.

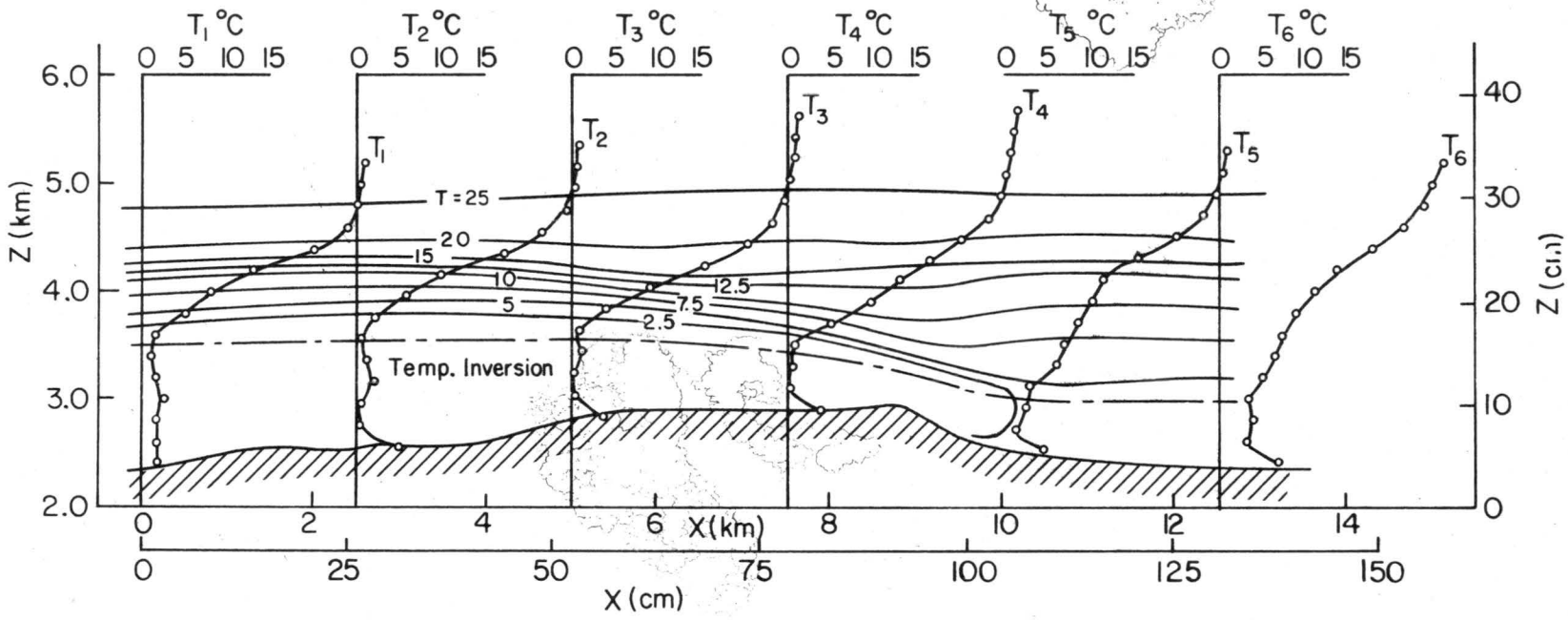

Fig. 15-1 Temperature profiles and isotherms along line B of laboratory model.

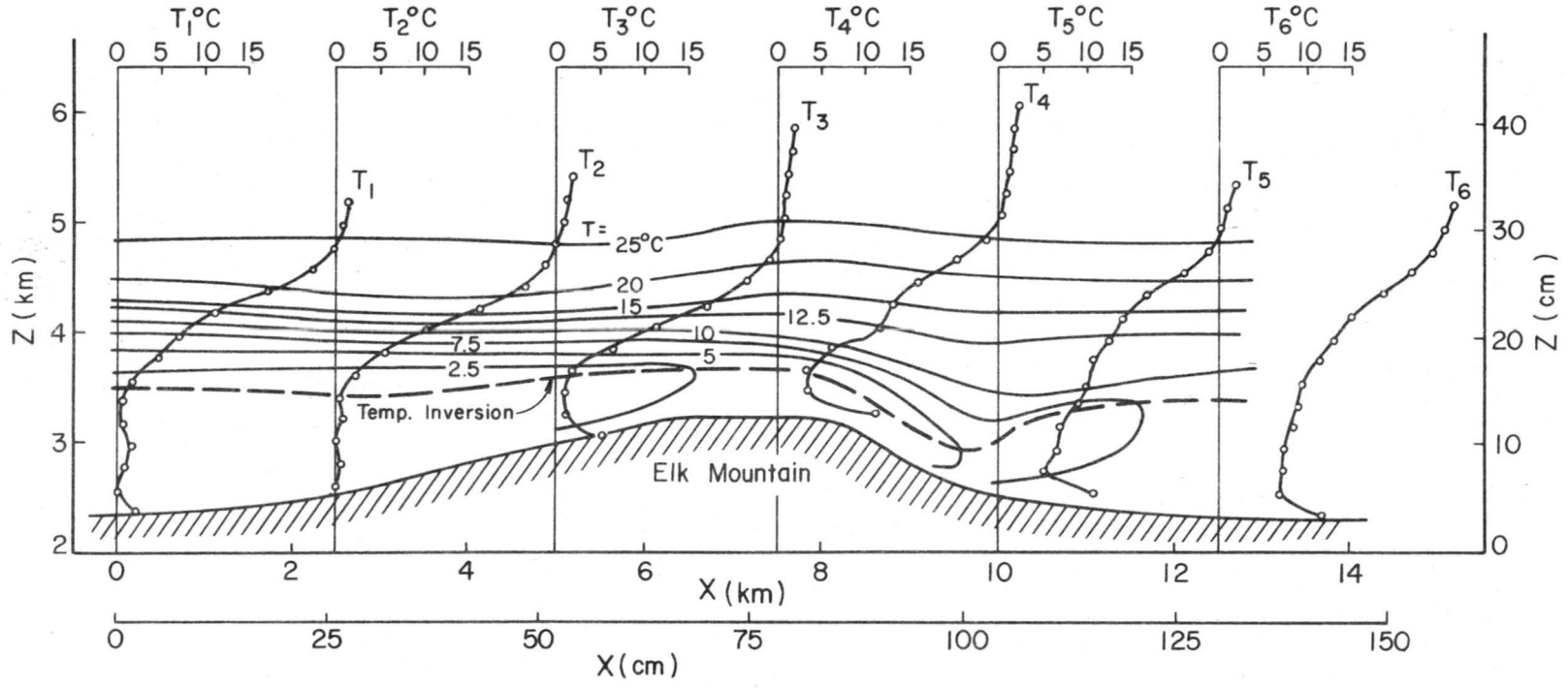

Fig. 15-2 Temperature profiles and isotherms along line C of laboratory model.

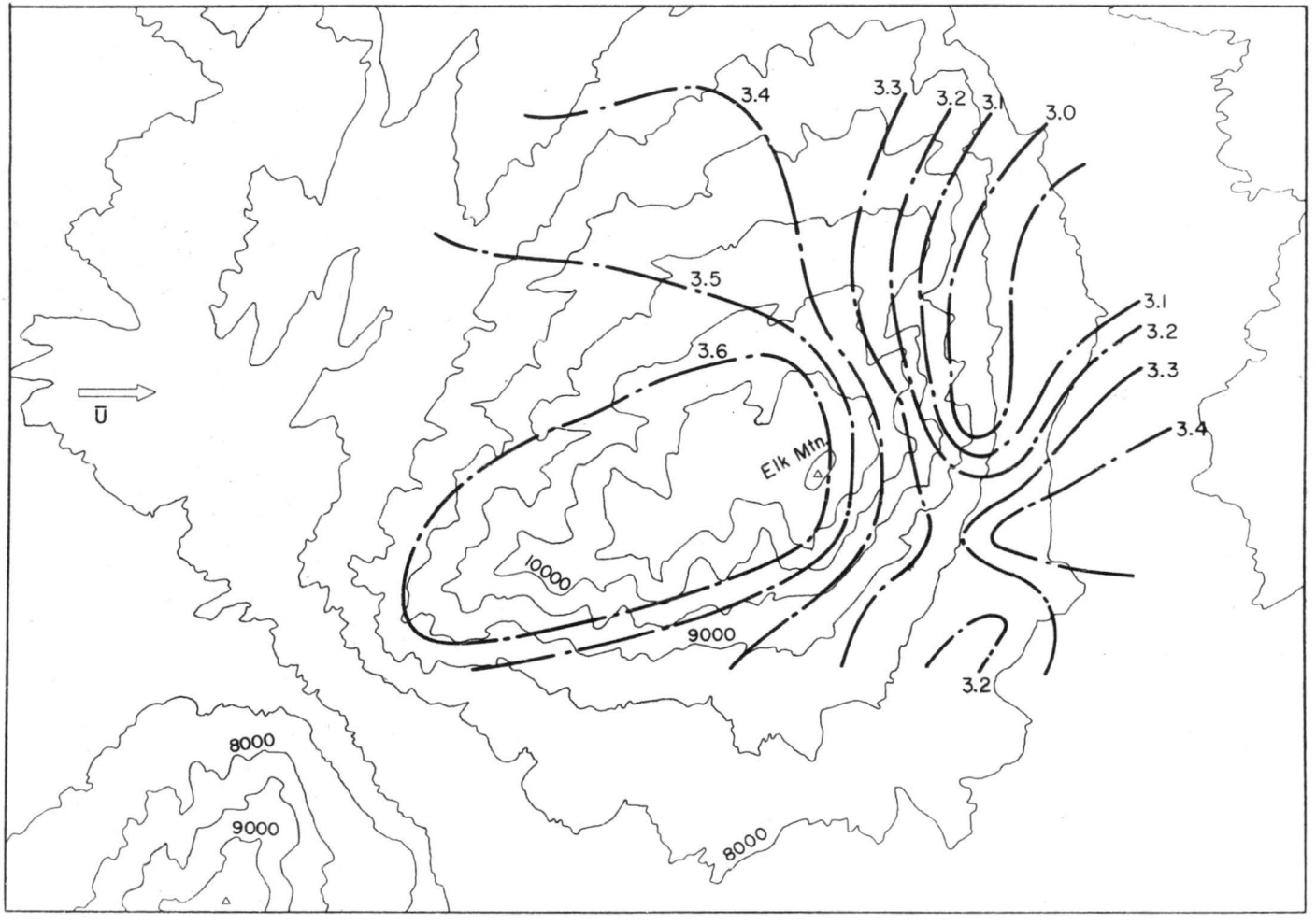

Fig. 16 The contour-lines of temperature inversion height over laboratory model (heights are in kilometer, scaled to prototype).

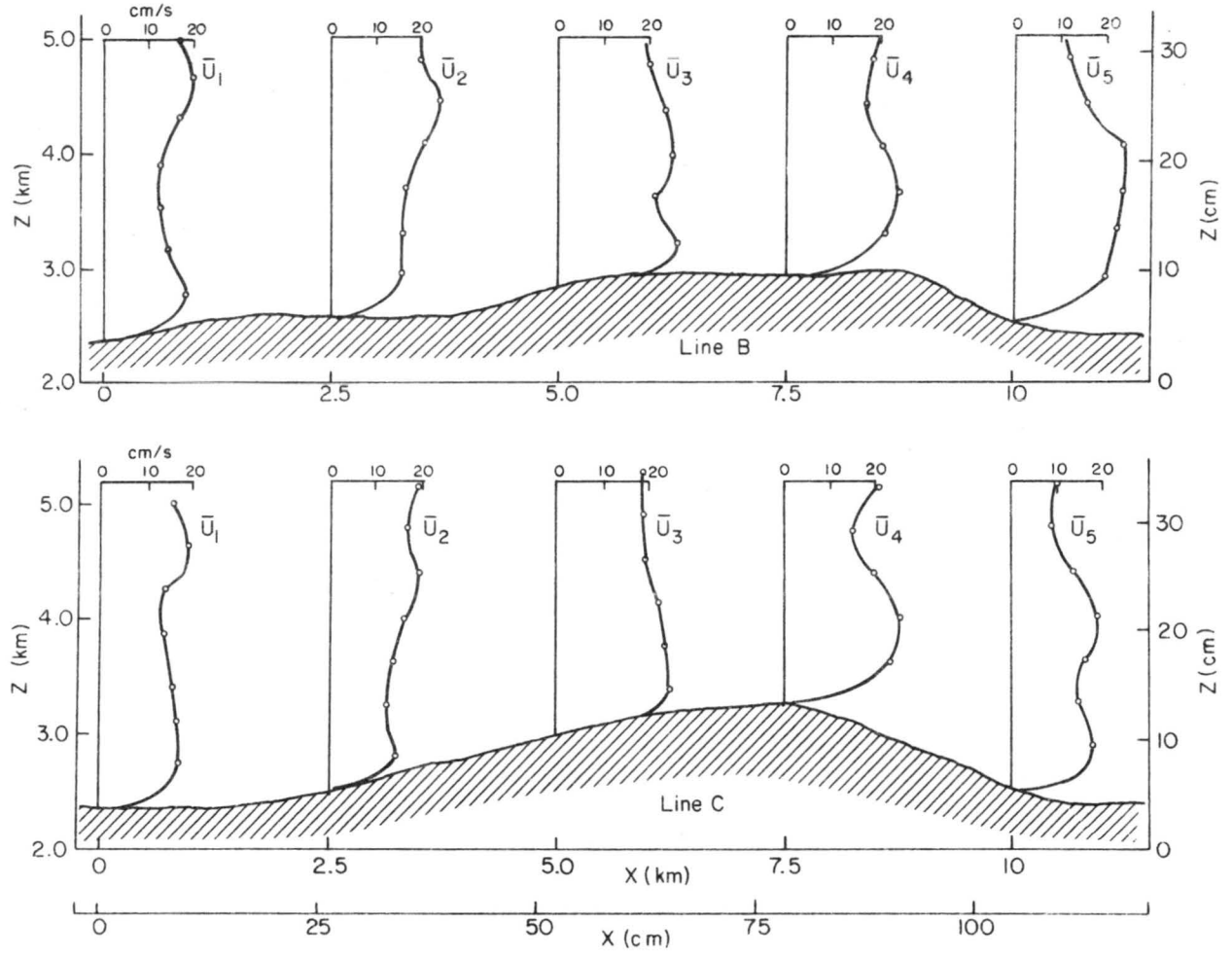

Fig. 17 Vertical profiles of wind velocity along lines B and C in stably-stratified airflow over laboratory model.

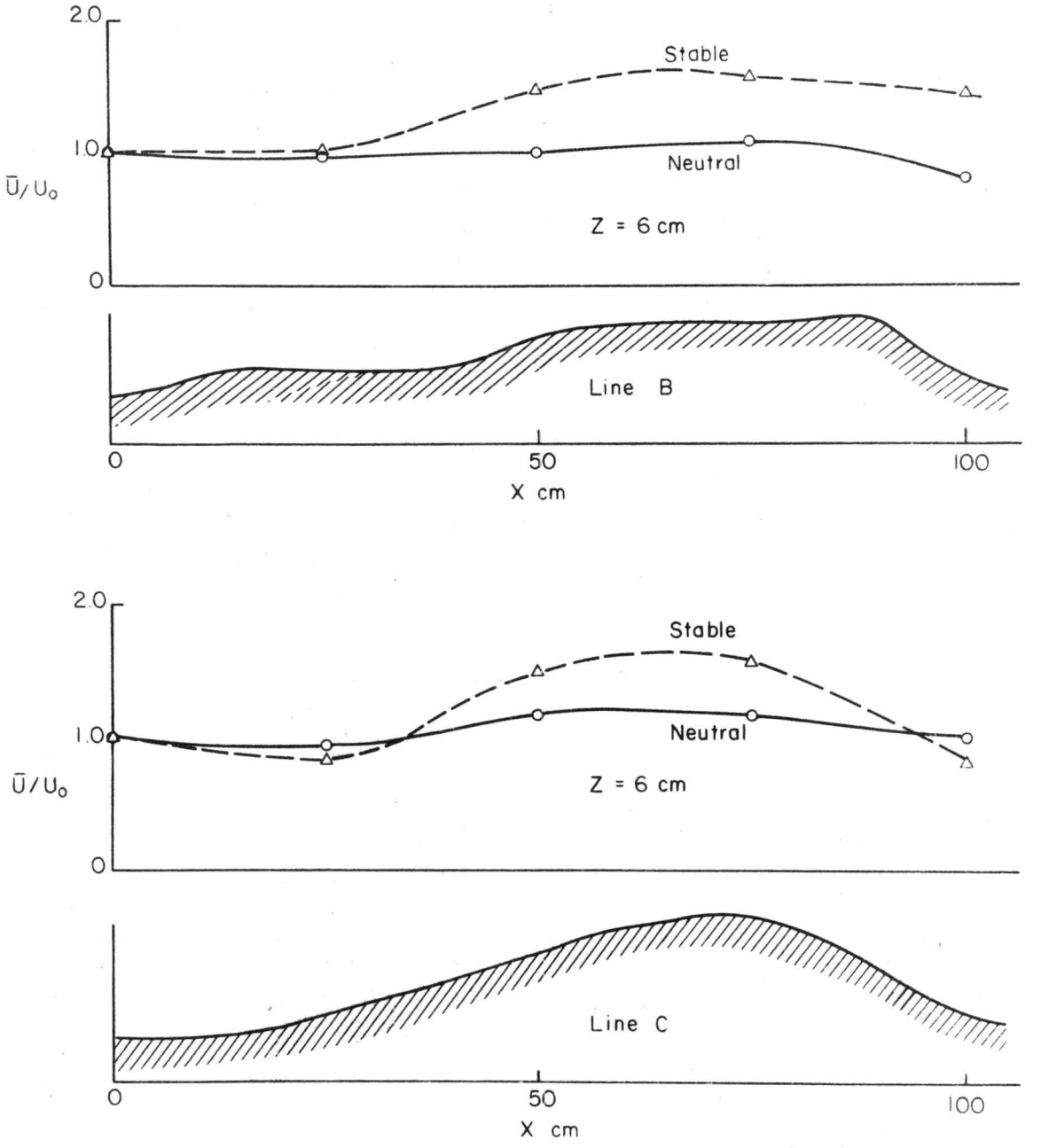

Fig. 18 Wind velocity distribution along lines B and C at height of 6 cm from the surface over laboratory model.

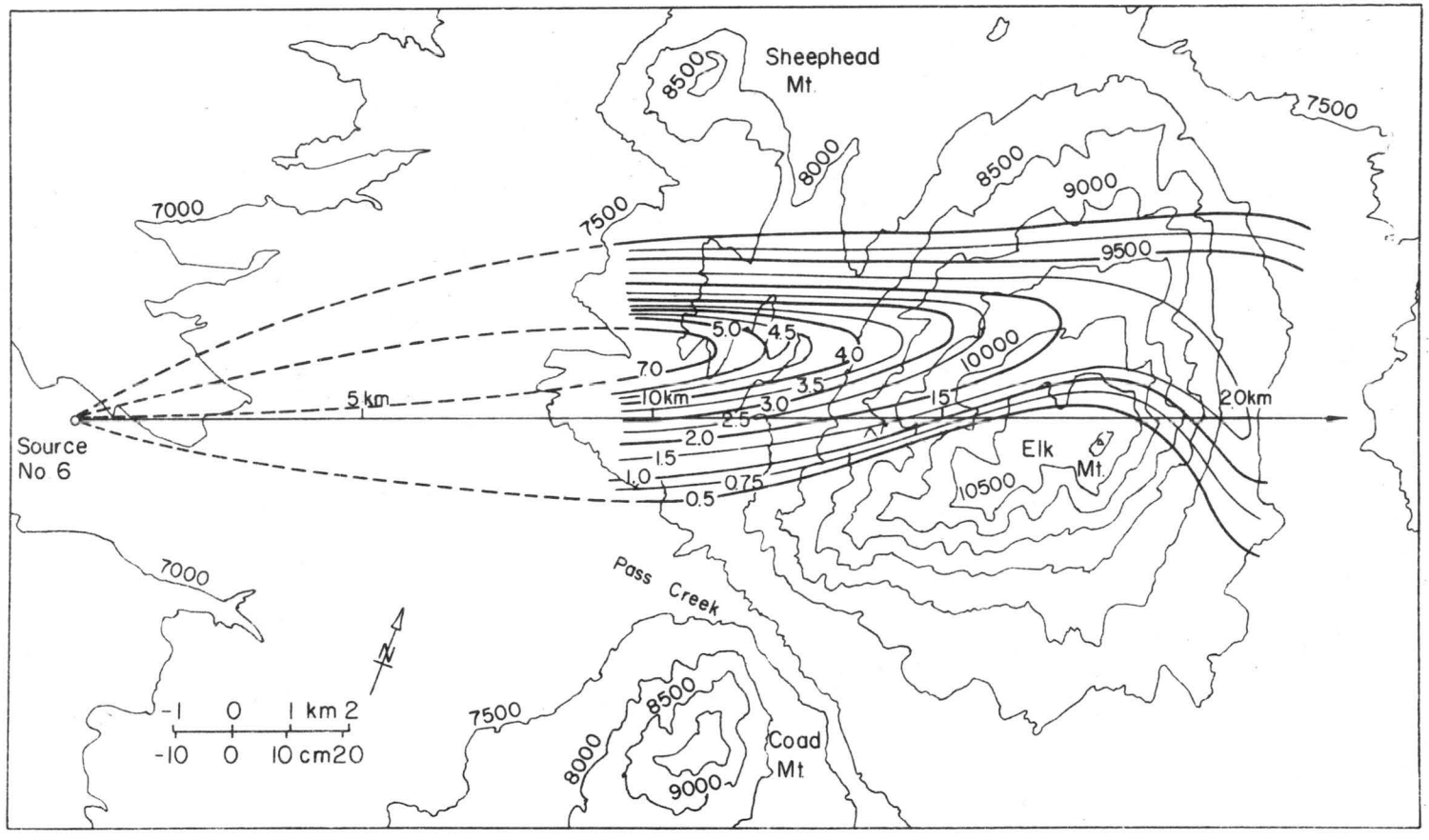

Fig. 19 Ground level contour lines of Krypton-85 in stably-stratified airflow over laboratory model. Concentrations are non-dimensionalized by $\frac{C\bar{U}h^2}{Q}$.

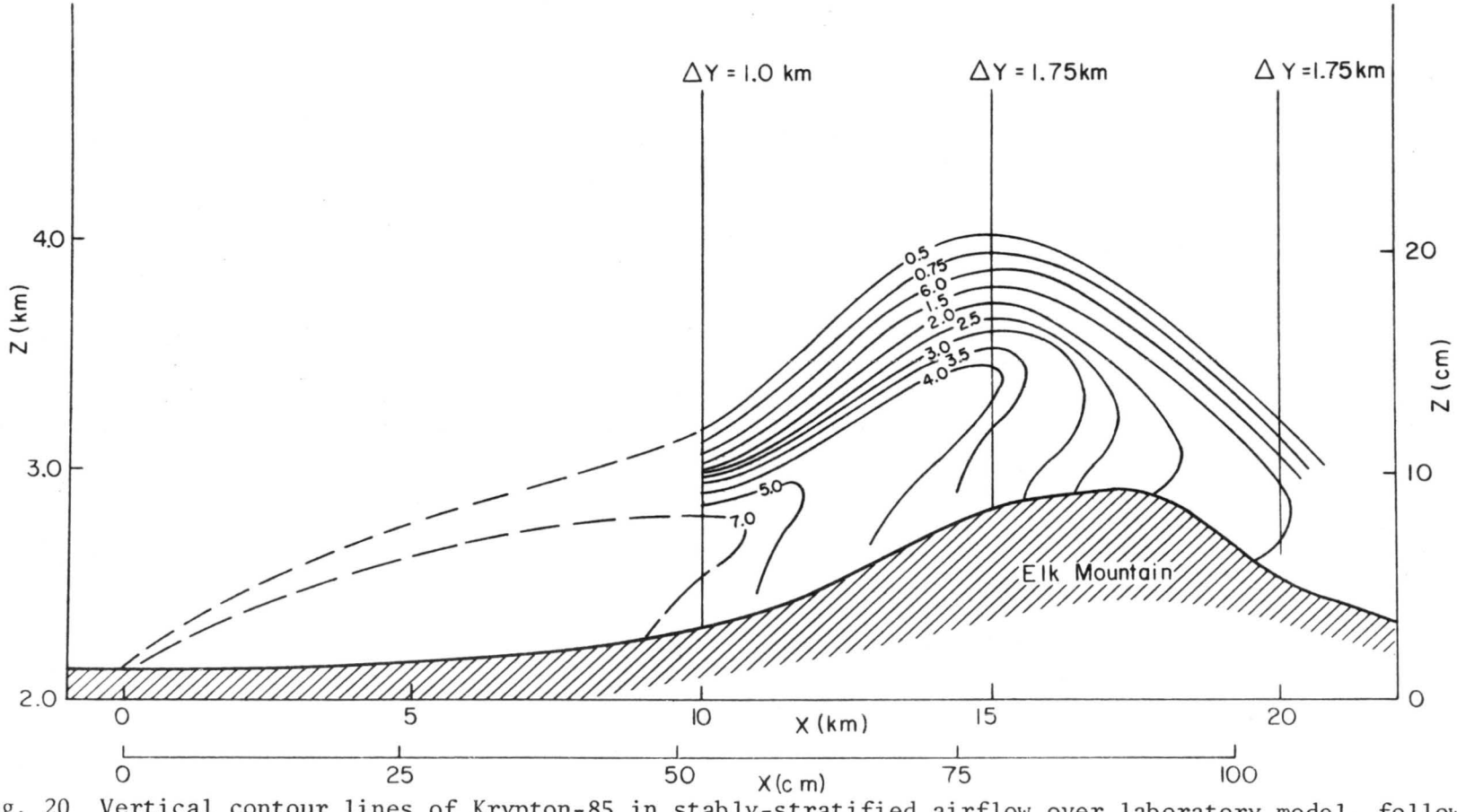

Fig. 20 Vertical contour lines of Krypton-85 in stably-stratified airflow over laboratory model, following trace of ground level maximum concentration. Numbers are non-dimensional concentration $\frac{C\bar{U}h^2}{Q}$.

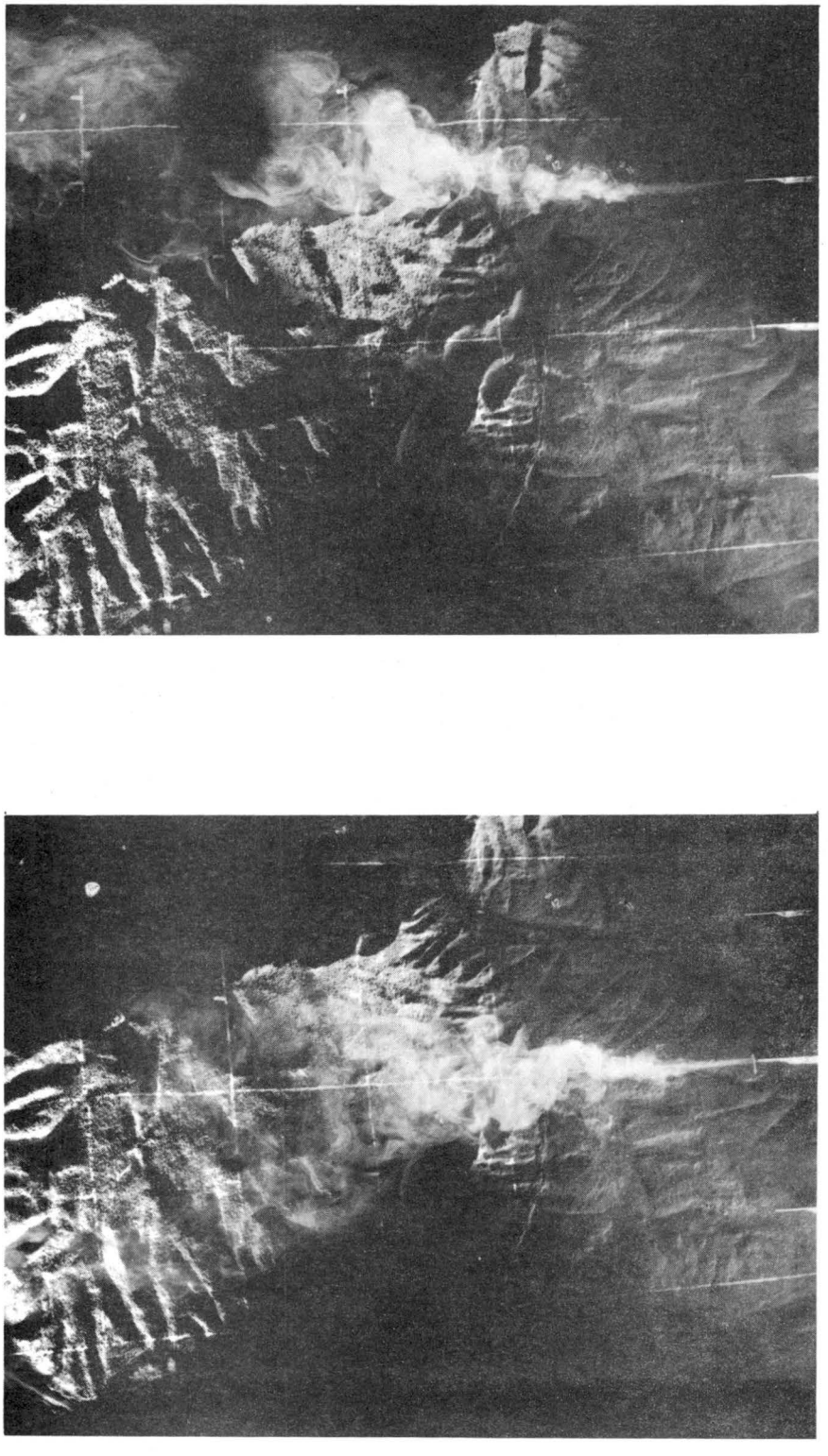

Fig. 21 Smoke flow in stably-stratified condition.

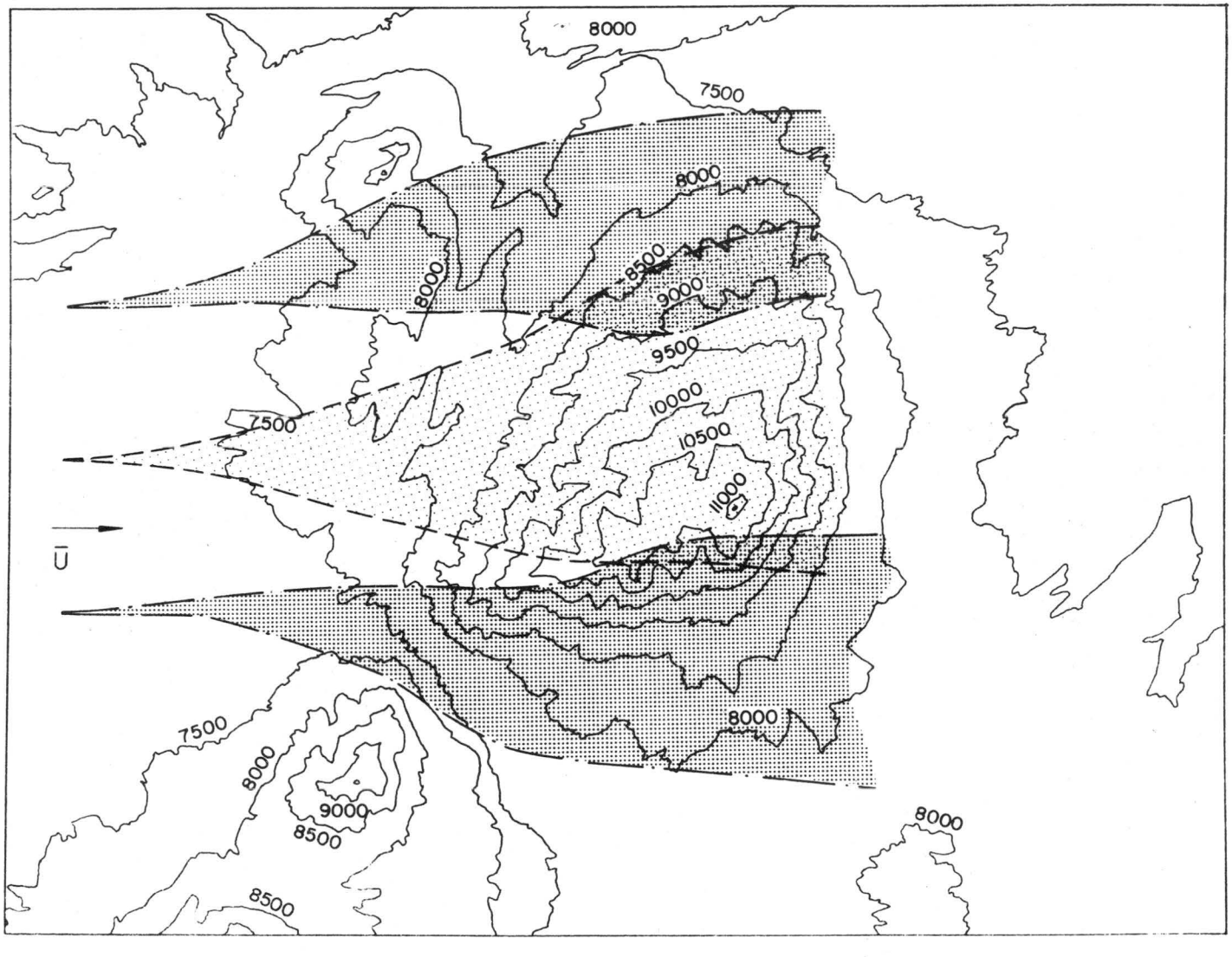

Fig. 22 Outline of smoke plume in stably-stratified airflow, defined from photographs of smoke.

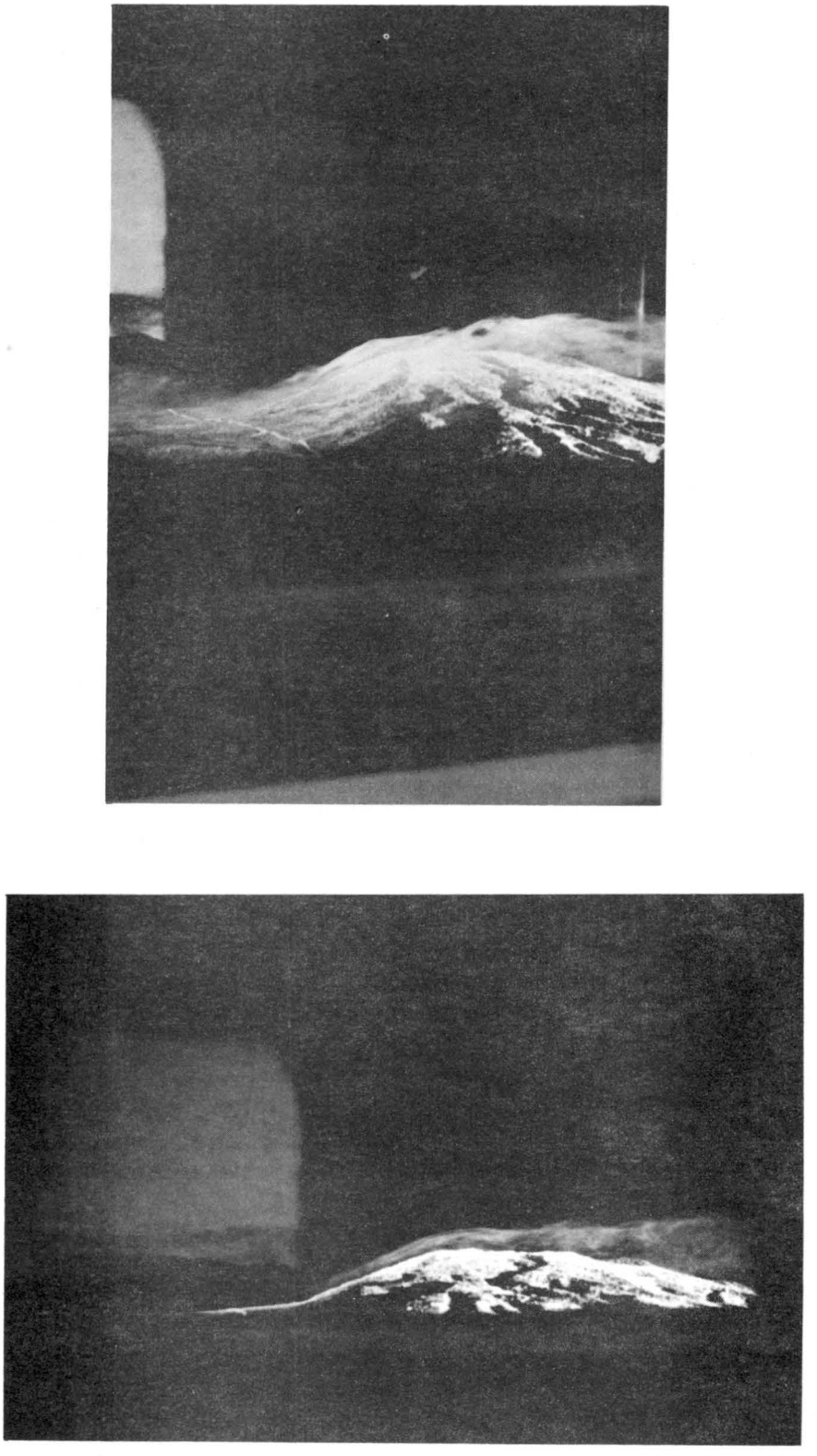

Fig. 23 Side view of smoke flow in wind tunnel (stably-stratified airflow).

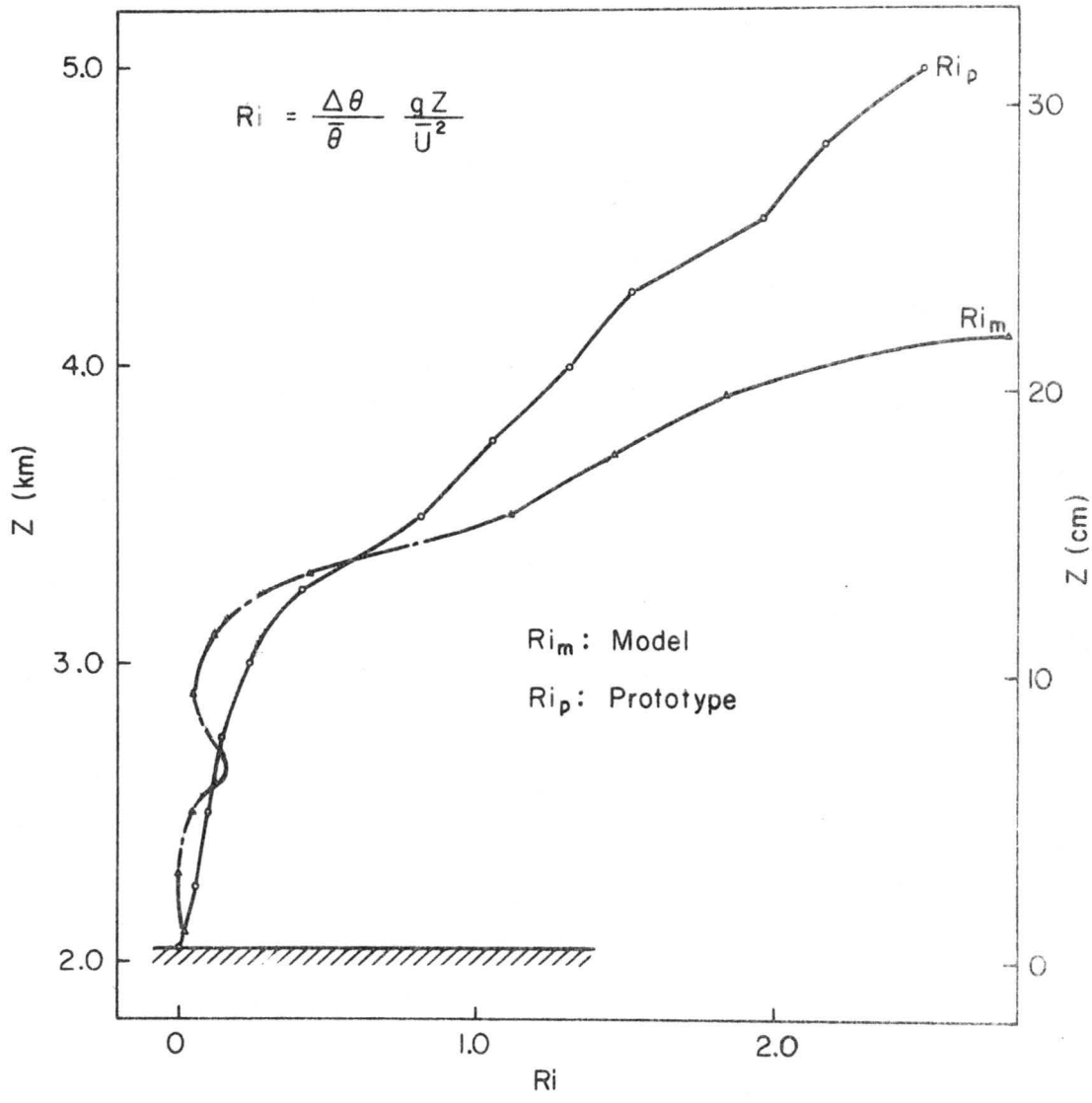

Fig. 24 Bulk Richardson number profiles in wind tunnel and in field calculated at the point 1-C for model and radar site for prototype.